MOUNTAIN-PLAINS CONSORTIUM

MPC 19-401 | N. Markosian, R. Thomas, M. Maguire, and A. Sorensen

Calcium Sulfoaluminate Cement Concrete for Prestressed Bridge Girders:Prestressing Losses, Bond, and Strength Behavior

MOUNTAIN-PLAINS CONSORTIUM REGION 8

A University Transportation Center sponsored by the U.S. Department of Transportation serving the Mountain-Plains Region. Consortium members:

Colorado State University
North Dakota State University
South Dakota State University
University of Colorado Denver
University of Denver
University of Utah
Utah State University
University of Wyoming

Technical Report Documentation Page

1. Report No.	2. Government Accession No.	3. Recipient's Catalog No.
MPC-560		

4. Title and Subtitle	5. Report Date
Calcium Sulfoaluminate Cement Concrete for Prestressed Bridge Girders:Prestressing Losses, Bond, and Strength Behavior	December 2019
	6. Performing Organization Code

7. Author(s)	8. Performing Organization Report No.
Nicholas A. Markosian Robert Thomas Marc Maguire Andrew Sorensen	MPC 19-401

9. Performing Organization Name and Address	10. Work Unit No. (TRAIS)
Utah State University 4110 Old Main Hill Logan, UT 84322-4110	11. Contract or Grant No.

12. Sponsoring Agency Name and Address	13. Type of Report and Period Covered
Mountain-Plains Consortium North Dakota State University PO Box 6050, Fargo, ND 58108	Final Report 1-1-2018 to 5-31-2019
	14. Sponsoring Agency Code

15. Supplementary Notes

Supported by a grant from the US DOT, University Transportation Centers Program

16. Abstract

Calcium sulfoaluminate (CSA) cement was used to cast a prestressed voided deck slab bridge girder. The rapid-set properties of CSA cement allowed the initial concrete strength to reach the required 4300 psi needed in order to cut the prestressing strands 6.5 hours after casting. Prestress losses were monitored long term using vibrating wire strain gages cast into the concrete at the level of the prestressing strands, and the data were compared to the American Association of State Highway and Transportation Officials Load and Resistance Factor Design (AASHTO LRFD) predictions for prestress losses. AASHTO methods for prestress loss calculation were overestimated compared with the vibrating wire strain gage data. Material testing was performed to quantify material properties, including compressive strength, tensile strength, static and dynamic elastic modulus, creep, and drying and autogenous shrinkage. The material testing results were compared with AASHTO predictions for creep and shrinkage losses.

The bridge girder was tested at midspan and a distance 1.25 times the depth of the beam from the face of the support until failure. Midspan testing consisted of a crack reopening test to solve for the effective prestress in the girder and a test until failure. The crack reopen effective prestress was compared with the AASHTO prediction, and AASHTO appeared to be effective in predicting losses based on the crack reopen data. The midspan failure was a shear failure, as accurately predicted by AASHTO. The 1.25d test resulted in a bond failure, which was accurately predicted by the AASHTO bond model for prestressed concrete.

17. Key Word	18. Distribution Statement
Calcium Sulfoaluminate Cement, Bridge Girders, prestressing steel bond, prestressing losses	Public distribution

19. Security Classif. (of this report)	20. Security Classif. (of this page)	21. No. of Pages	22. Price
Unclassified	Unclassified	84	n/a

Form DOT F 1700.7 (8-72) Reproduction of completed page authorized

Calcium Sulfoaluminate Cement Concrete for Prestressed Bridge Girders:Prestressing Losses, Bond, and Strength Behavior

Nicholas A. Markosian
Robert Thomas
Marc Maguire
Andrew Sorensen

Utah State University
Logan, Utah

December 2019

Acknowledgements

The support from the Mountain-Plains Consortium, CTS Cements, and Olympus Precast for funding, donation of time, and materials is acknowledged.

Disclaimer

ABSTRACT

Calcium sulfoaluminate (CSA) cement was used to cast a prestressed voided deck slab bridge girder. The rapid-set properties of CSA cement allowed the initial concrete strength to reach the required 4300 psi needed in order to cut the prestressing strands 6.5 hours after casting. Prestress losses were monitored long term using vibrating wire strain gages cast into the concrete at the level of the prestressing strands, and the data were compared to the American Association of State Highway and Transportation Officials Load and Resistance Factor Design (AASHTO LRFD) predictions for prestress losses. AASHTO methods for prestress loss calculation were overestimated compared with the vibrating wire strain gage data. Material testing was performed to quantify material properties, including compressive strength, tensile strength, static and dynamic elastic modulus, creep, and drying and autogenous shrinkage. The material testing results were compared with AASHTO predictions for creep and shrinkage losses.

The bridge girder was tested at midspan and a distance 1.25 times the depth of the beam from the face of the support until failure. Midspan testing consisted of a crack reopening test to solve for the effective prestress in the girder and a test until failure. The crack reopen effective prestress was compared with the AASHTO prediction, and AASHTO appeared to be effective in predicting losses based on the crack reopen data. The midspan failure was a shear failure, as accurately predicted by AASHTO. The 1.25d test resulted in a bond failure, which was accurately predicted by the AASHTO bond model for prestressed concrete. Funding for this project was provided by The Mountain Plains Consortium.

TABLE OF CONTENTS

LIST OF TABLES

LIST OF FIGURES

EXECUTIVE SUMMARY

The precast/prestressed concrete industry is always at the mercy of time. Time controls production and bed turnover rates, thus time can be the difference between winning a bid for a project versus losing the bid. As such, precast concrete contractors take many precautions to ensure that time is being used in the most efficient way possible. Some measures taken include the use of steam curing to speed up curing time, along with admixtures that allow the concrete to reach strength much faster.

Due to the growing need for increased turnover and production of precast/prestressed concrete, there is much need for research to speed up this process. The implementation of rapid setting concrete is one potentially sustainable alternative for use in precast/prestressed concrete. One such type of concrete uses calcium sulfoaluminate (CSA) cement to reach up to 50% of its ultimate strength in the first four hours (Thomas et al. 2018).

Because of its rapid setting qualities, CSA cement is currently used in repair work and patching of concrete roads and bridge decks. The application of CSA cement in prestressed concrete has particular appeal because that rapid set time is not as serious a logistical issue in the controlled environment of a precast concrete plant when compared with a ready-mix situation. The sustainability of CSA cement concrete also makes it an attractive alternative to Portland cement concrete because of the high carbon emissions involved in mining, transportation, and manufacturing of Portland cement concrete. In addition, sustainability in concrete production is important because concrete is the most mass produced building material in the world. Portland cement CO_2 emissions can be reduced by nearly 50% by using CSA cement concrete (Bowser 2016).

In this research, CSA cement concrete was used in the casting of a prestressed voided deck slab. In order to pour the concrete without the concrete setting, extensive lab mixing of CSA cement concrete was performed in order to find the desired combination of one-hour set time and initial concrete compressive strength of 4300 psi. The second phase of the study consisted of material property testing of the CSA cement concrete, which was performed in the laboratory at Utah State University. The third phase of this study was the prestress losses measurement and full-scale development length testing of the voided deck slab.

Effective prestress measured from the crack reopening test was 138.2 ksi, very close to the AASHTO value of 139.1 ksi.

For the destructive testing, the development length of the strand was investigated, maximum applied load at the midspan was 258 kips with a corresponding deflection of 2.096 in. measured directly beneath the load, and a shear failure was observed.

The maximum applied moment was 1,290 kip-ft., while strain compatibility predicted a value of 1,466.2 kip-ft. Based on this calculation, the observed shear failure (and its prediction) and the lack of slip during the test, the development length for the strand is less than the embedment length (132 in.) for the midspan test. A bond-slip failure occurred for the 1.25d test as made evident by the bond-model shown in Section 7.5. Bond stress capacity according to AASHTO is 104.35 ksi, compared with the test-implied maximum stress of 256.96 ksi in the strand. General recommendations are that the AASHTO code can adequately predict behavior of CSA cement concrete bridge girders with attention paid to prestress loss prediction, and would be a viable option for increasing bed turnover in precast plants and reducing CO_2 emissions within the industry.

1. INTRODUCTION

1.1 Overview

The precast/prestressed concrete industry is always at the mercy of time. Time controls production and bed turnover rates, thus time can be the difference between winning a bid for a project versus losing the bid. As such, precast concrete contractors take many precautions to ensure that time is being used in the most efficient way possible. Some measures taken include the use of steam curing to speed up curing time, along with admixtures that allow the concrete to reach strength much faster.

Due to the growing need for increased turnover and production of precast/prestressed concrete, there is much need for research to speed up this process. The implementation of rapid setting concrete is one potentially sustainable alternative for use in precast/prestressed concrete. One such type of concrete uses calcium sulfoaluminate (CSA) cement to reach up to 50% of its ultimate strength in the first four hours (Thomas et al. 2018).

CSA cement is currently used in repair work and patching of concrete roads and bridge decks because of its rapid setting qualities. The application of CSA cement in prestressed concrete has particular appeal because that rapid set time is not as serious a logistic issue in the controlled environment of a precast concrete plant when compared with a ready-mix situation. Precast concrete fabricators have a much more optimized and timely process for mixing, traveling, and pouring concrete than that of cast-in-place concrete.

The sustainability of CSA cement concrete also makes it an attractive alternative to Portland cement concrete because of the high carbon emissions involved in mining, transportation, and manufacturing of Portland cement concrete. In addition, sustainability in concrete production is important because concrete is the most mass produced building material in the world. Portland cement CO_2 emissions can be reduced by nearly 50% by using CSA cement concrete (Bowser 2016). One-third of the carbon emissions can be reduced in the production process, with additional reductions coming from the lack of need for mined raw materials (Bescher et al. 2012).

1.2 Objectives

The main objectives of this study were to study the effects of implementing CSA cement concrete into precast/prestressed concrete, as well as test the plausibility of actually using Rapid Set© cement in a precast/prestressed concrete plant. The specimen provided for testing was a voided deck slab cast at Olympus Precast in Bluffdale, Utah. An extensive testing program was required before, during, and after the concrete pour in order to fully understand the effects of using CSA cement.

1.2.1 Material Testing Program

Testing has two major components: material properties and structural behavioral testing. The material properties tested included compressive strength, split tensile strength, static and dynamic modulus, creep, drying shrinkage, autogenous shrinkage, set time, and maturity. Compressive, tensile, and modulus tests were performed at various time intervals in order to derive the full strength development curve up to 28 days for the CSA cement concrete. The tests from the day of the pour were duplicated in the lab at Utah State University by graduate and undergraduate research assistants.

The structural tests consisted of transfer length, strand end-slip, and camber measurements. Transfer length was measured by mounting detachable mechanical strain gages (DEMECs) to the deck of the voided deck slab directly above the prestressing strand. Camber measurements were taken by taking measurements with an engineer's level and a high precision (0.1 mm) steel ruler at various locations along the length of the beam.

1.3 Thesis Organization

This thesis is divided into eight chapters. Chapter 1 introduces the goals and background information of this research project. Chapter 2 provides an extensive literature review covering CSA cement chemical structure, prestressed concrete measurement techniques, prestressed concrete design methodologies, and prestressed concrete definitions and applications. Chapter 3 summarizes experimental testing methods. Chapter 4 summarizes material testing results from laboratory material testing. Chapter 5 summarizes prestress losses as measured compared with AASHTO predicted values. Chapter 6 summarizes the results of the midspan testing as compared with predicted AASHTO capacities for shear and moment. Chapter 7 summarizes the testing at 1.25d and compares it with AASHTO predicted capacities for shear and moment. Chapter 8 summarizes the study and provides conclusions and further needs for research regarding CSA cement concrete in prestressed concrete members.

2. LITERATURE REVIEW

2.1 Transfer Length

Prestressed concrete members are formed by tensioning steel strands and pouring concrete around the strands once the strands are tensioned to the desired load. This load, often measured in units of stress, is called the effective prestress. After the concrete has cured and reached the specified strength, the steel strands are cut either by means of a flame torch while tension is still being applied, or by slowly releasing the tension in the strands and cutting the strands (Carroll 2009).

Prestressed concrete members rely on bond stresses between the steel strands and the concrete to act as a composite member. The transfer bond in a pretensioned concrete beam occurs near the end of the member and anchors the effective prestress force directly between the prestressing steel strands and the concrete (Cross 2012). The length required for this bond to fully develop is called the transfer length.

2.1.1 Measuring Transfer Length

It is important to understand the transfer length in prestressed members because the chemical bond between the strands and the concrete has no effect along the transfer length, sometimes also referred to as the transfer zone (Janney 1954). Transfer length can be measured by using detachable mechanical strain gages (DEMECs) mounted onto the concrete surface and measuring the change in surface strain to estimate the transfer length. Theoretically, the transfer length is equal to the length along the prestressed member where the surface strains are changing. The change in surface strain levels off eventually, and this point can be estimated as the transfer length. Another way to measure transfer length is to measure strand end-slip and use the measured value along with some equations for approximating transfer length developed in previous research (Carroll 2009).

Transfer length is not readily measured in the typical way for voided deck slab sections and other uncommon shapes because the formwork does not allow DEMECs to be attached to the concrete at the level of the prestressing strand. Therefore, in order to measure transfer length for voided slab beams and other sections, the DEMECs can be attached to the top flanges of the beams, directly above the prestressing strands (Maguire 2009).

Strands also have a tendency to slip near the ends of the member in prestressed concrete right after transfer. This is called strand end-slip and can be measured to estimate transfer length. Strand end-slip measurements are an easy way to estimate transfer length because the process is much simpler than surface strain measurements, but it can be less reliable for estimating transfer length (Carroll 2009).

As the strand is released, there is a tendency for it to slip against the concrete, but is resisted by the mechanical interlock between the steel and the concrete and the increased frictional force from the strand's tendency to increase in diameter after release, or the Hoyer Effect (Cross 2012). There is, however, strand slip along the transfer length until a full bond has been developed. Strand end-slip measurements are taken by averaging a distance measured from the end of the member to a fixed point on the strand both before and after prestress transfer. An equation for calculating strand end-slip is given below.

$$\Delta_{es} = l_i - l_f \tag{2.1}$$

Where:

Δ_{es} = strand end-slip (in.)
l_i = average of measurements prior to transfer (in.)
l_f = average of measurements taken after transfer (in.)

Transfer length can be calculated from strand end-slip measurements by using Guyon's formula (Guyon 1960). The formula makes use of Hooke's law and assumes the strain in the strand just prior to release is equal to the stress in the strand just prior to release divided by the elastic modulus of the prestressing strand. Therefore, Guyon's formula for transfer length is reduced to the following equation.

$$l_t = \alpha \frac{E_{ps}}{f_{ps}} \Delta_{es} \tag{2.2}$$

Where:

$\alpha = 2$
E_{ps} = Modulus of Elasticity of prestressing strand (psi)
f_{ps} = Stress in prestressing strand just prior to transfer (psi)
Δ_{es} = Strand end-slip measurement (in.)

2.1.2 Estimating Transfer Length

Transfer length can be estimated using equations developed for the ACI 318 and AASHTO codes. There are two equations for estimating transfer length in the ACI 318 and AASHTO codes, which are shown below.

$$l_t = \frac{f_{se}}{3} \times d_b \tag{2.3}$$

Where:

l_t = transfer length (in.)
f_{se} = effective prestress (ksi)
d_b = diameter of the prestressing strands (in.)

This equation is used in the sixth edition of the PCI design manual as the transfer length portion of PCI equation 4.2.3.1. This equation can be simplified with an assumed effective prestress of the strands of 150 ksi, and is given below (Carroll 2009).

$$l_t = 50 d_b \tag{2.4}$$

Where l_t and d_b are as defined in the above paragraph. There are other equations that have been proposed for transfer length based on research, but this paper will compare the previous equations with actual measured values.

2.2 Prestress Losses

Before prestress transfer can occur, the prestress force is anchored mechanically by use of hydraulic jacks to steel abutments on opposite ends of a casting bed. The end of the strand jacked by the hydraulic jacks is called the live or jacking end, and the end attached to the abutment is called the dead end. The axial stress in the prestressing strands causes the diameter of the strands to decrease due to Poisson's effect (Maguire 2009).

When the prestressing strands are cut to allow for transfer of the prestress force, the axial tension in the strands is released and turned into a compressive force on the concrete. The release of the pretensioning tends to cause the strands to return to their original diameter. The effective prestress in prestressed concrete members may decrease over time. This phenomenon is known as prestress loss. There are many sources of prestress loss in a prestressed concrete member that are time related, and many that can occur immediately or just after transfer (cutting the prestressing strands).

2.2.1 Time Dependent Effects

Time related prestress losses occur due to the nonlinear behavior of concrete over time. Shrinkage and creep over time result in a loss of strain and a shorter strand length in the member, which in turn results in lower stress (Cross 2012). Strands also have a tendency to relax over time independent of strain changes, which also results in a decrease in the effective prestress of the strands. Creep, relaxation, and concrete shrinkage all lead to changes in the magnitude of prestress over the life of a prestressed member (Pettigrew 2014).

2.2.2 Measuring Prestress Loss

Prestress losses are measured using vibrating wire strain gages (VWSG) attached to the prestressing strands and cast into the concrete. The strain gages are connected to a data acquisition system, which measures the change in strain before and after transfer. Using material properties and the change in strain, prestress losses in the strands can be measured. Data are also collected throughout the curing process. The effective prestress can also be back-calculated by way of crack initiation tests (Cross 2012).

Crack initiation tests consist of incrementally loading the beam until the first crack is observed, unloading the beam, and placing a strain gage over the crack in order to measure the flexural strain in the concrete. A line of DEMEC gages can also be used to compare the concrete surface strain at the location of initial crack opening. The DEMEC gages should be placed at a location as close as possible to the centroid of the prestressing steel, with measurements taken before and after loading to calculate the change in surface strain. However, a line of DEMEC gages as close to the bottom fiber of the beam as possible will allow for quicker recognition of crack formation.

Crack reopening tests can be performed after the crack initiation test, with the ultimate goal of determining the load that cracks formed in the initiation test begin to reopen. A strain gage spans the crack and plots strain data to a data acquisition system to determine the point at which the member no longer performs linearly.

2.2.3 Estimating Prestress Loss

There are two methods for prestress loss calculations provided in AASHTO design codes. The refined method uses the equation given below and is based on research from Tadros et al. (2003). Sources of instantaneous loss due to applied loads include loss due to prestress application and self-weight at transfer as well as superimposed dead loads from deck installation (Cross 2012).

$$\Delta f_{pT} = \Delta f_{pES} + \Delta f_{pLT} \tag{2.5}$$

Where:

Δf_{pT} = total prestress loss (ksi)

Δf_{pES} = prestress loss from elastic deformations due to instantaneously applied loads (ksi)

Δf_{pLT} = prestress loss due to the effects of creep, relaxation, and shrinkage (ksi)

Equations for Δf_{pES} and Δf_{pLT} are given below.

$$\Delta f_{pES} = \frac{E_p}{E_{ct}} f_{cgp} \tag{2.6}$$

Where:

E_p = modulus of elasticity of prestressing steel (ksi)
E_{ct} = modulus of elasticity of concrete at transfer or time of load application (ksi)
f_{cgp} = concrete stress at the center of gravity of prestressing tendons due to the prestressing force immediately after transfer and the self-weight of the member at the section of maximum moment (ksi)

$$\Delta f_{pLT} = 10.0 \frac{f_{pi} A_{ps}}{A_g} \gamma_h \gamma_{st} + 12.0 \gamma_h \gamma_{st} + \Delta f_{pR} \tag{2.7}$$

Where:

f_{pi} = prestressing steel stress immediately prior to transfer (ksi)
A_{ps} = area of prestressing steel (in.^{2})
A_g = gross area of section (in.^{2})
γ_h = 1.7-0.1H, correction factor for relative humidity of air
$\gamma_{st} = \frac{5}{(1-f'_{ci})}$, correction factor for specified concrete strength at time of prestress transfer to the concrete member

Prestress losses may also be calculated by multiplying the elastic modulus of the prestressing steel by the measured change in strain of the prestressing strand (Barr et al. 2008).

2.3 Camber

Prestressed concrete members often have strands located below the neutral axis. When these strands are pretensioned, the force in the strands creates an eccentric load on the member cross section. This eccentricity causes an initial upward deflection of the member immediately after release. This initial upward deflection is called camber. Although the member self-weight counteracts the effects of the upward camber, the net deflection generally follows the camber due to the eccentric load on the cross section (Kassner 2012).

Concrete has a tendency to creep over time. This creep, which acts in the opposite direction as the camber, often tends to increase the camber over time. The change in camber over time is called camber growth. It is important to estimate camber correctly because an over-prediction of camber can result in excessive deflections. The excess deflections lead to a need for an increased concrete deck thickness, which also negatively affects the deflections. This problem becomes cyclical, as more deflections require more concrete, and more concrete leads to more deflections (Cross 2012).

The time-dependency of camber due to creep affects the constructability, based on the difference in time between pouring, delivery, and erection of the structure. Camber is also affected by the thermal loading during construction, independent of the actual load on the member. Difficulties arise in measuring camber due to thermal gradients and differential shrinkage of concrete. Understanding and accurately predicting camber is very important in creating a successful, safe, and economical structural system.

2.3.1 Measuring Camber

Camber growth is typically monitored by way of the taut wire method, which involves stringing a 12-gauge steel piano wire over pulleys at the end of the member and fixing a ruler to the actual member. Rulers and mirrors are placed on the beam at the ends, quarter points, and midspan of the specimen. The mirrors help to prevent parallax, which can skew the readings based on the angle between the reader's eye and the wire (Carroll 2009). Readings are taken by lining up the actual wire with its reflection on the mirror and reading that point from the ruler. Camber measurements are taken before prestress transfer, immediately after prestress transfer, and at regular intervals after curing.

In certain cases, the forms cannot be removed before the strands are cut, meaning that the taut-wire method may not be used. In replacement, the use of an engineer's level is used to measure the change in elevation of the top surface of the member.

2.3.2 Estimating Camber

Initial camber can be estimated using provisions in AASHTO Article 5.7.3.6, which can be taken as:

$$\uparrow^{+}\ \Delta_{i/p} = \frac{P_{rel} e_{tr} L^2}{8 E_{ci} I_{tr}} \tag{2.8}$$

Where:

$\Delta_{i/p}$ = initial deflection due to prestressing (in.)
P_{rel} = prestress force prior to release (kips)
e_{tr} = strand eccentricity with respect to transformed concrete section, taken positive below centroid (in.)
L = beam length (in.)
E_{ci} = concrete elastic modulus at release (ksi)
I_{tr} = moment of inertia of the transformed concrete section (in.^{4})

However, this equation does not account for the creep of the concrete due to the self-weight of the concrete. The deflection due to the self-weight of the beam, if the self-weight is considered to be uniformly distributed, can be found from basic mechanics as:

$$\uparrow^{+}\ \Delta_{i/sw} = -\frac{5 w_{sw} L^4}{384 E_{ci} I_{tr}} \tag{2.9}$$

Where:

$\Delta_{i/sw}$ = initial deflection due to beam self-weight (in.)
w_{sw} = beam self-weight (kip/in.)

Therefore, initial camber in a beam with straight strands and subjected only to its own self-weight can be taken as:

$$\uparrow^{+}\ \Delta_i = \Delta_{i/p} + \Delta_{i/sw} = \frac{P_{rel} e_{tr} L^2}{8 E_{ci} I_{tr}} - \frac{5 w_{sw} L^4}{384 E_{ci} I_{tr}} \tag{2.10}$$

Time-dependent camber can be estimated using prestress losses due to creep, shrinkage, and other time-related effects. Camber growth can be estimated using two categories of methods: deflection multiplier and refined. The multiplier method was used in this paper to compare the actual long-term camber measured from the voided deck slab. Long-term camber using the multiplier method consists of

calculating the initial deflections due to self-weight and the prestress force and multiplying the initial deflection by a multiplier from PCI Design Manual, 7th Edition, given in Table 2.1.

Table 2.1 PCI Simple Span Long-Term Camber Multipliers

	Without Composite Topping	With Composite Topping
At Erection:		
(1) Deflection (downward) component-apply to the elastic deflection due to the component weight at release of prestress	1.85	1.85
(2) Camber (upward) component-apply to the elastic camber due to prestress at the time of release of prestress	1.80	1.80
Final:		
(3) Deflection (downward) component-apply to the elastic deflection due to the component weight at release of prestress	2.70	2.40
(4) Camber (upward) component-apply to the elastic camber due to the prestress at the time of release of prestress	2.45	2.20
(5) Deflection (downward)-apply to elastic deflection due to superimposed dead load only	3.00	3.00
(6) Deflection (downward)-apply to elastic deflection caused by the composite topping	----	2.30

2.4 Development Length

Bond stresses are formed between the concrete and steel prestressing strands due to the tensile force created from flexure (Cross 2012). In order for the beam to begin cracking due to flexure, relative slip between the concrete and steel strands must occur. The flexural bond stress near the crack increases considerably just after cracking. The length over which the flexural bond occurs from the end of the transfer length to the embedment length is called the development length (Carroll 2009). Development length can also be defined as the minimum length of embedment required to develop the nominal moment capacity of the member.

2.4.1 Bond Stresses

Bond stresses in pretensioned concrete members can be affected by several factors, including strand surface conditions, strength of the concrete, cross-section of the strands, cross-section of the member, time-related creep, and a few others (Maguire 2009). Steel strands with rust or epoxy with grit can develop transfer lengths much shorter than strands with clean, smooth surfaces. Higher strength concrete can also form a better frictional and mechanical bond with the strands due to the higher bond stress imposed by the concrete on the steel strands (Cross 2012). The size of individual strands can also change the transfer and bond lengths. In strands with larger diameters, the force in each strand is larger for a given stress due to the increase in cross-sectional area. Therefore, the length required to develop the transfer and development lengths increases with the diameter of the strands (Carroll 2009). Larger cross-sections of concrete members are able to withstand stresses better when the strands are released, which can reduce the transfer length of the specimen. Time-dependent effects such as creep may occur over time, and transfer lengths have been measured to be shorter over time (Cross 2012). Type of loading, strand spacing, concrete cover, confinement, strand casting position, and consolidation within the transfer zone have also been known to affect transfer and development lengths.

2.4.2 Measuring Development Length

As the development length consists of the transfer length and the minimum flexural bond length, transfer lengths must be known before testing. Flexural tests are used to find the flexural bond length, and the bond length is added to the transfer length in order to find the development length.

2.4.3 Estimating Development Length

AASHTO LRFD specifications for development length of pretensioned concrete members can be taken as:

$$l_d = \mathrm{K}(f_{ps} - \frac{2}{3} f_{pe}) d_b \tag{2.7}$$

Where:

l_d = development length (in.)

K = 1.6 for prestressed members with depth greater than 24 in., 1.0 otherwise

f_{ps} = average stress in prestressing steel at the time for which nominal resistance is required (ksi)

f_{pe} = effective stress in the prestressing steel considering losses (ksi)

d_b = nominal strand diameter (in.)

2.5 Shear Capacity of Prestressed Members

Shear capacity of prestressed concrete members can be calculated in multiple ways. According to ACI 318 and Equation 5-20 to 5-24, shear capacity is equal to the sum of the shear capacity in the steel and the shear capacity in the concrete. The shear capacity in the concrete is taken as the lesser of the two equations below added to the steel shear capacity:

$$V_{ci} = 0.6\lambda\sqrt{f'_c} b_w d + \frac{V_i M_{cre}}{M_{max}} + V_d \tag{2.8}$$

$$V_{cw} = \left(3.5\sqrt{f'_c} + 0.3 f_{pc}\right) b_w d + V_p \tag{2.9}$$

Where:

V_{ci} = flexure shear cracking (kips)

V_{cw} = web shear cracking (kips)

f_{pc} = longitudinal stress at centroid of the cross-section due to all loads (ksi)

b_w = width of the web (in.)

d = the maximum of the distance from the extreme compressive fiber to the centroid of the prestressed reinforcement, or 0.8h (in.)

V_i = factored shear due to all loads (kips)

M_{cre} = shear cracking moment (kip-in.)

M_{max} = factored moment due to all loads (kip-in.)

V_d = unfactored shear due to all loads (kips)

V_p = vertical component of prestressing reinforcement (kips)

AASHTO provides similar equations for shear capacity using V_{ci}/V_{cw}. All variables are as defined above in the ACI 318 equation for shear. The minimum of the calculated V_{ci} and V_{cw} is used for the V_c value in Equation 2.12, which corresponds to AASHTO Equation 5.8.3.3-1. The minimum of Equation 2.12 and 2.13 is taken as the nominal shear resistance of the member, V_n.

$$V_{ci} = 0.02\sqrt{f'_c}b_w d + \frac{V_i M_{cre}}{M_{max}} + V_d \geq 0.06\sqrt{f'_c}b_w d \tag{2.10}$$

$$V_{cw} = \left(0.06\sqrt{f'_c} + 0.3f_{pc}\right) b_w d + V_p \tag{2.11}$$

$$V_n = V_c + V_s + V_p \tag{2.12}$$

$$V_n = 0.25 f'_c b_w d + V_p \tag{2.13}$$

Modified compression field theory (MCFT) accounts for the actual angle that shear cracks form, which can be considerably less than 45°, and thus gives a more accurate prediction. MCFT also accounts for the average principal stresses in the cracked concrete. Figure 2.1 gives the equations used in MCFT.

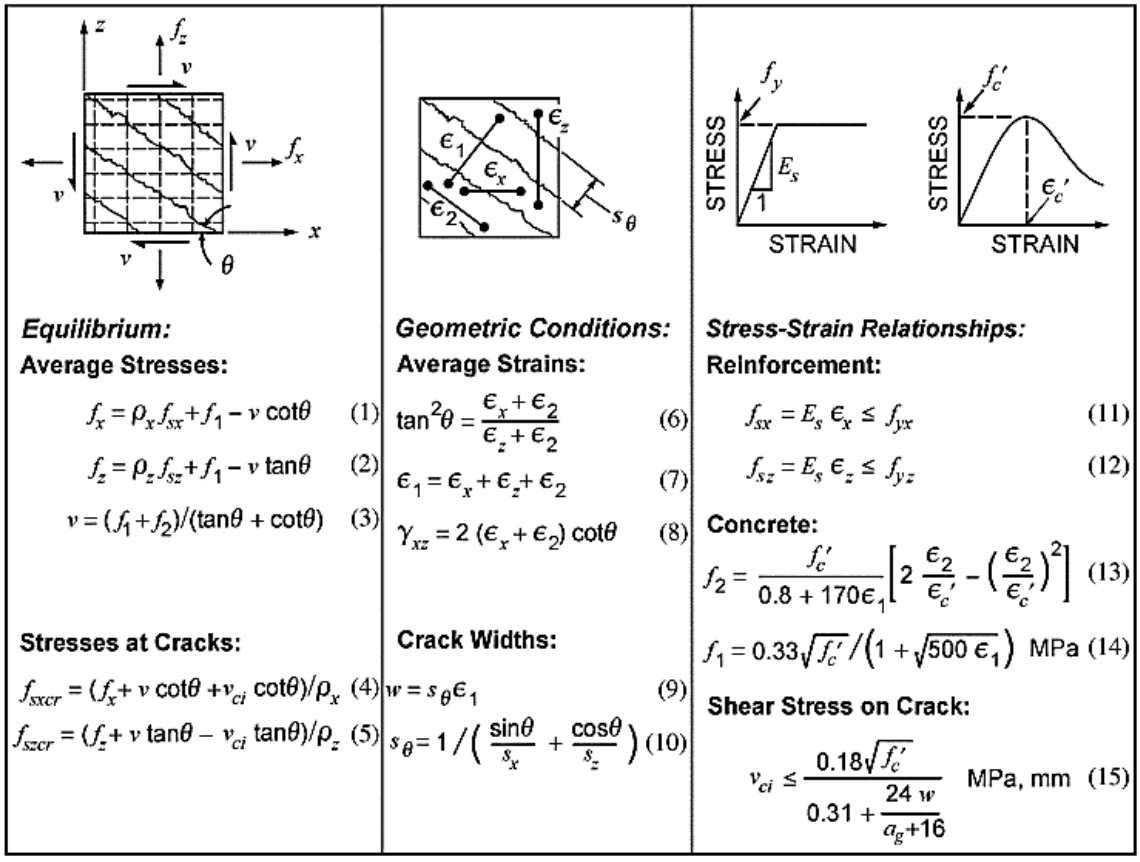

Figure 2.1 Modified Compression Field Theory Equations

The third shear capacity calculation this paper will summarize comes from Bentz et al. (2006), who came up with a simplified version of MCFT that is accurate for a wide range of concrete sections, but much simpler to use and more general. The equations below summarize how to solve for shear stress in a concrete member.

$$v = v_c + v_s = \beta\sqrt{f'_c} + \rho_z f_y cot\theta \tag{2.14}$$

Where:

v = total shear stress (psi)

v_c = shear stress in the concrete (psi)

v_s = shear stress in the steel (psi)

f'_c = compressive strength of concrete (psi)

$\beta = \frac{33cot\theta}{1+\sqrt{500\varepsilon_1}} \leq \frac{2.17}{0.31+24w(a_g+16)}$

a_g = maximum coarse aggregate size (mm)

ε_1 = principle tensile strain

$\rho_z = \frac{A_v}{b_w s}$ = ratio of stirrup area to web area

f_y = yield strength of the shear reinforcement (psi)

$\theta = (29\,\text{deg} + 7000\varepsilon_x)\left(0.88 + \frac{s_x}{100}\right) \leq 75\ deg$

Several researchers have tested the shear capacity of Portland cement concrete girders (Eder et al. 2005, Maguire et al. 2013, Pettigrew et al. 2016).

2.6 Calcium Sulfoaluminate Cement

Calcium sulfoaluminate (CSA) cements were first introduced around 1960 and have been produced on an industrial scale in China since the 1970s (Thomas et al. 2018). Although these cements have been produced in mass amounts in China for nearly 50 years, CSA cements have only recently been introduced in North America as high-early-strength alternatives to Portland cement.

CSA cements also offer a potentially sustainable alternative to traditional Portland cements because of their chemical composition, lack of need for raw materials, and lower carbon emissions produced during manufacturing (Bescher et al. 2012). The added benefit of sustainability goes a long way in making CSA cements an attractive alternative to traditional Portland cements because concrete is the most widely manufactured building material worldwide.

2.6.1 CSA Cement Concrete in Use at SEA-TAC Airport

CSA cements are known for their rapid set times, which can gain up to 50% of their ultimate strength in as little as four hours without the use of steam curing (Bowser 2016). This high-early-strength property of CSA cements makes them an ideal choice for use in patchwork on concrete that requires high early strength. One famous project involved repaving at the SEA-TAC airport in Seattle in 1995. According to Bescher et al. (2012), the airport could only close for four hours, so the repave mix had to reach adequate compressive strength during those hours the airport could be closed. Because of the high repeated live loads, the concrete mix needed to also perform with high durability. The mix was designed for a 20-year design life, which was equivalent to 1,150,000 MD-11 aircraft movements.

Flexural beam specimens were cast using the mix for the paving, and fatigue testing was done on the beam specimens until failure. The fatigue tests helped determine the minimum compressive strength of the concrete needed to accommodate the 20-year design life. Using the assumptions for calculating the fatigue performance of the pavement, it was determined that the CSA cement concrete could actually accommodate nearly 4.5 billion MD-11 departures. Perhaps the most important discovery from these tests was that even if the CSA cement concrete stopped gaining strength at four hours, it would still be able to accommodate 60 times the initial design life of 20 years. Durability of CSA cement concrete makes it an even more attractive alternative to Portland cement concretes.

2.6.2 Chemical Composition of CSA Cement Concrete

The chemical composition of CSA cement is very different from that of traditional Portland cement. The oxide composition of Portland cement is predominantly formed from calcium oxide (CaO), silica (SiO_2), and to a lesser extent, alumina (Al_2O_3). These oxides show up in the form of alite (C_3S), belite (C_2S), aluminate (C_3A), and ferrite (C_4AF). CSA cements are richer in alumina and poorer in calcium oxide and silica than Portland cement, and sulfate (SO_3) is also abundant in CSA. Ye'elimite (C_4A_3S), belite, ferrite, and calcium sulfate exhibit these oxides in CSA cements. Calcium sulfate is often ground into CSA clinker from gypsum or anhydrite at 15% to 20% by mass, compared with the 3% to 5% added to Portland cement clinker. Ettringite ($C_6A\hat{S}_3H_{32}$), amorphous aluminate, and monosulfate ($C_4A\hat{S}H_{18}$) are the main reaction products. (Thomas et al. 2018)

Setting time for CSA cements are extremely short due to the rapid crystallization of the ettringite in hydration. At low water dosages, the initial setting time can be as short as 10 minutes. Colder temperatures and higher water-to-cement ratios lead to longer working time. Many different kinds of acids have been found to be effective retardants for CSA cement, including citric boric, gluconic, and tartaric acids (Zajac et al. 2016). Setting times can be delayed as long as one hour with the right admixture proportions, cooler mixing temperatures, and the right amount of water, but are still difficult to reach.

2.6.3 Sustainability

The application of CSA cement concrete can increase the sustainability of concrete products in multiple ways. CSA cement has lower embodied energy than Portland cement because it is produced with mostly recycled materials as opposed to the virgin limestone required to produce traditional Portland cement (Thomas et al. 2018). The use of recycled materials reduces the resource consumption of CSA cement production by about 60%, as compared with Portland cement production.

In addition, pyro processing energy is greatly reduced due to (1) inclusion of high volumes of synthetic gypsum and (2) lower clinker temperature than Portland cement. The clinkering process in CSA cement requires around 200℃ to 250℃ lower burning temperatures than Portland cement (Winnefield 2009). Carbon footprint reduction is a very good way to tell if an alternative is sustainable, or at least more environmentally friendly than traditional building material. CSA produces about 600 kg of CO_2 for every 1,000 kg of cement produced, compared with roughly 900 kg of CO_2 for every 1,000 kg of Portland cement produced (Bescher et al. 2012).

The carbon footprint of CSA cement production can also be reduced because industrial waste materials can be used in production, instead of mining and transporting new alumina and bauxite. Industrial waste that can be used in CSA cements includes calcium sulfate wastes from hydrofluoric acid production or power plant scrubbers (Bescher et al. 2012). Total carbon emissions for production of CSA cements are reduced by 30% to 50% because of the lower quantities of calcium oxide in the clinker phase of CSA cement (Thomas et al. 2018).

2.7 Application of CSA Cement in Prestressed Concrete

The implementation of CSA cement in precast/prestressed concrete has the potential to increase bed turnover rates and production and allow for greater sustainability in the precast concrete industry. The rapid-setting properties of CSA cement concrete almost disqualify it for use as structural cast-in-place concrete, as long workability times are necessary for successful concrete mixes. Precast concrete plants tend to provide much more controlled conditions for pouring concrete, and most have an on-site batch plant, so the rapid-setting time is not as much of an issue as it is for cast-in-place concrete. Although the

rapid-setting time is not as big an issue in precast concrete, the need for good workability is still necessary in order to successfully pour the concrete and keep it from setting up in the concrete truck.

Bowser et al. (2016) set out to use CSA cement concrete in prestressed bridge girders to compare the effects of prestress losses, transfer length, and development length. The CSA cement concrete bridge girders were compared to a control group of traditional Portland cement concrete girders of the same dimensions and reinforcement. Prestress losses are measured using vibrating wire strain gages embedded in the concrete and attached to the prestressing strands. The transfer lengths were measured using DEMECs attached to the concrete at the level of the prestressing strands. The measured lengths were then compared to the expected values from the ACI and AASHTO design provisions for transfer length. The prestressing strands were cut at two hours and the transfer lengths were measured. Transfer lengths were well approximated by ACI and overestimated by the AASHTO provisions. The prestress losses measured in all CSA beams were consistent, but the AASHTO equations for prestress loss vastly overestimated the prestress losses measured in the beams by upwards of 50%.

3. EXPERIMENTAL METHODS

3.1 Introduction

Due to the relatively unknown behavior of CSA cement concrete, an extensive testing program was developed in order to understand the behavior. The material testing program is broken up into four phases: 1) mix design, 2) day of concrete pour testing, 3) laboratory mix replication, and 4) full-scale specimen testing. Each of the four phases is described in depth in this chapter.

3.2 Mix Design

Because of the lack of experience with CSA cement, multiple trial mixes were required in order to perfect the set time, compressive strength, and workability. Because of the quickness with which CSA cement sets, it was important to provide enough time and workability in the mix to allow for the concrete to be mixed at the batch plant, placed in the concrete truck, driven to the pour site, and placed in the forms without setting.

In order to begin the mix design, recommended ratios for cement, water, aggregates, and admixtures were taken from CTS Cement, the manufacturer of CSA cement used for this project. Initially, five trial mixes were made in order to determine the right water-to-cement ratio, amount of superplasticizer, and amount of retarder. After five batches were made, the final mix design reached the goal compressive strength of 5000 psi at four hours and a set time of about one hour.

This mix design was discovered to be flawed during lab mixing as the initial mixes used expired cement. When replicated with fresh CSA cement bags in the lab, the mix design flash set in the mixer. The mixing procedure needed to be altered in order to activate the retarder admixture. As recommended by CTS Cement, the mixing procedure was changed by adding around 50% of the water with all admixtures mixed into the aggregates before adding the cement, and the remaining water/admixtures after the cement was added. This allowed the admixtures to evenly distribute throughout the mix and be more effective, especially in retarding the set time. It was also recommended to remove fly ash from the mixture, as it has been known to cause issues with some chemical admixtures. After removing the fly ash from the mix and increasing the retarder by nearly 300%, an acceptable mix design was found and is shown in Table 3.2.1, given in units per cubic yard of concrete. The final mix design used a water-to-cement ratio of 0.40.

Table 3.1 Final Mix Design Proportions

CSA Mix Proportions		
CSA	700	**lb/cy**
WATER	280	**lb/cy**
COARSE	1650	**lb/cy**
FINE	1150	**lb/cy**
AIR	6	**%**
ADVACAST	98	**oz/cy**
DARAVAIR	52.5	**oz/cy**
RECOVER	182	**oz/cy**

Upon batching the concrete during the voided slab pour, it was found that the concrete was not as workable as the laboratory mixtures, and it was decided to add more water to the mixer and concrete truck. A total of 200 lbs, or 40 lb/yd^3, were added to the mixture in order to allow for the proper

workability needed to pour the concrete. The added water increased the water-to-cement ratio to 0.457, a 15.7% increase in water.

3.3 Day of Pour Concrete Testing

The extensive testing program for the day of the concrete pour was designed to give an understanding of a full spectrum of concrete behaviors. During the concrete pour, 50 cylinders, four thermally insulated cylinders, three autogenous shrinkage tubes, and three drying shrinkage prisms were filled with fresh concrete and prepared according to each respective ASTM standard. Slump, unit weight, and set time tests were performed throughout the duration of the pour. Once the concrete had set and begun to gain strength, detachable mechanical strain gages (DEMECs) were attached to the top surface of the slab, camber measurements were taken using an engineer's level, and strand end-slip measurements were taken before and after transfer using a depth micrometer.

3.3.1 Cylinder Compression Testing

Initially, the cylinder testing was meant to include 24 compression tests, 12 splitting tension tests, and 12 elastic modulus tests. Each test would be performed three specimens at a time every hour until the desired strength was achieved. After arriving at Olympus Precast, testing was limited to compression and dynamic elastic modulus tests, with a total of 50 specimens prepared according to ASTM C39. Compressive tests were done in a Forney testing machine, similar to the model in the concrete lab at Utah State University. Figure 3.1 shows the Forney testing machine at Utah State University.

Figure 3.1 Forney Compressive Testing Machine

3.3.2 Dynamic Elastic Modulus Testing

In addition to compressive tests, each cylinder tested on the day of the concrete pour was also tested using an NDT James Instruments Emodumeter for dynamic elastic modulus, as seen in Figure 3.2.

3.3.3 Set Time

Set time test specimens were created on the day of the pour. Set time specimens consisted of 6 in. x 12 in. cylinders cut in half and filled with mortar. The fresh concrete was filtered through a No. 20 sieve to ensure the set time specimens consist of only mortar. Set time penetration resistance tests were performed in accordance with ASTM C403 and measured using a Humboldt Acme Penetrometer, as shown in Figure 3.3.

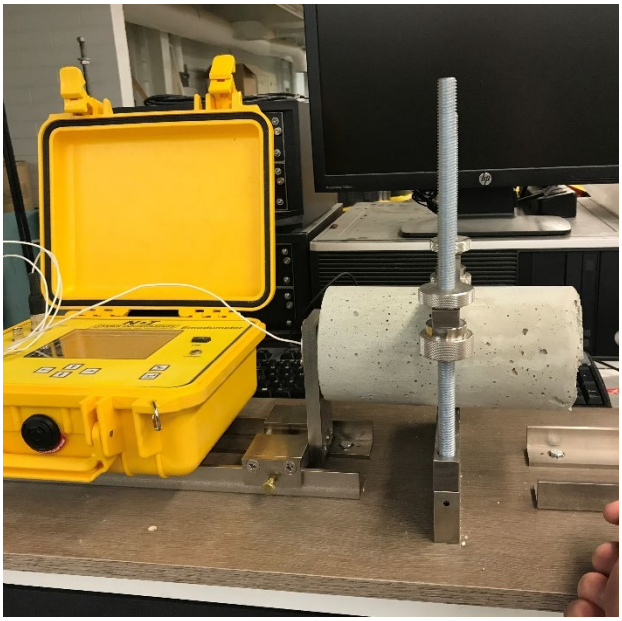

Figure 3.2 NDT Emodumeter Test Setup

Figure 3.3 Humboldt Acme Penetrometer

3.3.4 Drying Shrinkage

Three drying shrinkage prisms were made and placed in steel forms with gauge studs cast into the concrete. Initial measurements began when final set occurred and continued over the course of the day at the precast plant. Drying shrinkage prisms were prepared and tested in accordance with ASTM C596. Drying shrinkage molds are shown in Figure 3.4, and the shrinkage frame is shown in Figure 3.5.

Figure 3.4 Drying Shrinkage Molds

3.3.5 Autogenous Shrinkage

In addition to drying shrinkage prisms, three autogenous shrinkage tubes were filled with mortar that had been filtered through a No. 20 sieve. Autogenous shrinkage measurements were taken every 10 minutes after final set for one hour, then every 20 minutes for one hour, and once an hour until leaving the precast plant. Autogenous shrinkage tubes were prepared and tested in accordance with ASTM C1698. Figure 3.6 shows an autogenous shrinkage tube in the frame.

Figure 3.5 Drying Shrinkage Frame

Figure 3.6 Autogenous Shrinkage Test Setup

3.3.6 Laboratory Mix Replication

In order to create repeatable results, laboratory mixes were made in an attempt to replicate the as-cast mixture, considering the addition of extra water and the observed partial contamination with Portland cement. There was additional testing done to study the effects of creep on CSA cement concrete, as well as static elastic modulus tests and splitting tensile strength tests. Multiple concrete mixes were made as the mixing drum was limited to batch sizes of around 2 ft^3. At least six cylinders were made to compare compressive strengths across the different batches at two hours and four hours.

Figure 3.7 Color Comparison of Cylinder Molds

Due to the coloration and slower strength development of the concrete cylinders made on the day of the Olympus Precast pour, it was assumed that some small amount of Portland cement was present in the CSA cement silo. At first it was assumed that 10% Portland cement by weight was present for the initial laboratory replication mix. Figure 3.7 shows the color of the Olympus Precast concrete and a cylinder made with 100% CSA cement concrete. The cylinder on the left is from the Olympus pour and the cylinder on the right is made with 100% CSA cement concrete. A series of two more laboratory mixes were made with 5% and 2.48% Portland cement replacement in order to replicate the behavior of the cylinders made at Olympus Precast.

3.3.6.1 Compressive Strength Lab Tests

Each mix made was placed in the lab to test compressive strength every hour on the hour beginning at two hours and ending at six hours. Three cylinders were tested at each time interval. An increased 0.457 water-to-cement ratio was used in the concrete mixes to match the mix of the actual beam, as opposed to the initial mix design with a water-to-cement ratio of 0.40. Aggregates were used at saturated surface dry (SSD) conditions. All cylinders were tested in accordance with ASTM C39 for compressive strength of concrete in the Forney compressive testing machine, as seen in Figure 3.1.

3.3.6.2 Splitting Tensile Strength Lab Tests

Splitting tensile strength was measured in accordance with ASTM C496/C496-17. Limitations on the day of the concrete pour did not allow for the testing of splitting tensile strength, so only laboratory testing was used for the development of tensile strength. Due to the length of time required to perform one tensile strength test, cylinders were tested continuously beginning at two hours and continuing until six hours. Time of breaking and peak load were recorded for each test. Six compressive tests were also performed at two and four hours, to compare compressive strengths between mixes. Splitting tensile strength test setup is shown in Figure 3.8.

3.3.6.3 Static and Dynamic Elastic Modulus Tests

Static and dynamic elastic modulus testing was done in accordance with ASTM C469/C469M-14 and ASTM E1876-15, respectively. Due to time constraints and testing equipment limitations, only dynamic elastic modulus tests were done on the day of the voided deck slab pour. Therefore, comparisons between static and dynamic elastic modulus will be made using only the static elastic modulus tests in the laboratory. Static elastic modulus testing was done with a calibrated Tinius Olson universal testing machine and a compressometer attached to the cylinder, as seen in Figure 3.9. Dynamic elastic modulus testing was done with an NDT James Instruments Emodumeter, as seen in Figure 3.2.

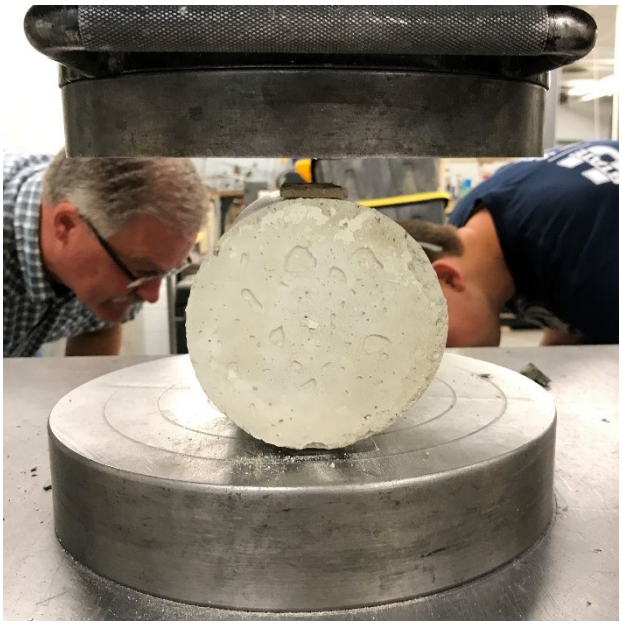

Figure 3.8 Splitting Tensile Strength Test Setup

3.3.6.4 Set Time, Autogenous Shrinkage, and Drying Shrinkage

Set time, autogenous shrinkage, and drying shrinkage were performed in the lab in the same manner as discussed in Section 3.3.2. All specimens were stored in a temperature controlled room after final set occurred.

Figure 3.9 Static Elastic Modulus Test Setup

3.3.6.5 Creep

Creep tests were performed in the laboratory according to ASTM C512 in a temperature controlled room. Three full-sized 4 in. x 8 in. cylinders and two half-height 4 in. x 8 in. cylinders were capped according to ASTM C617 and stacked on top of each other in a frame and held under a constant load of up to 40% of concrete compressive strength. Creep testing began four hours after casting of the cylinders and continued for 28 days. Strain measurements were taken in accordance with ASTM C512. The creep frame and test setup is shown in Figure 3.10.

3.3.7 Full-Scale Specimen Testing

In addition to laboratory concrete mix replication, a series of full-scale tests on the voided deck slab bridge girder were conducted. DEMEC measurements were taken in order to estimate transfer length of the voided deck slab. Camber measurements were also taken every two days up to 14 days, again at 28 days, and just before testing. Crack initiation, crack reopen, development length, and shear tests were performed on the full-scale voided deck slab.

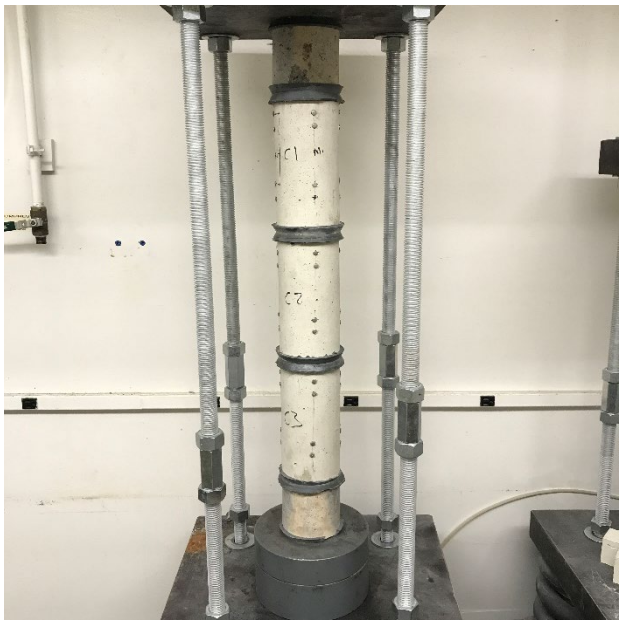

Figure 3.10 Creep Frame Test Set Up

3.3.7.1 Transfer Length

Concrete surface strain measurements were taken using DEMECs and calipers accurate to the nearest thousandth of an inch. DEMECs were placed on both the live and dead ends of the voided deck slab, beginning 2 inches from the end of the member and continuing at 4-in. spacing for 60 inches. DEMEC placement is shown in Figure 3.11. Figure 3.12 shows the calipers used for measuring concrete surface strains. All measurements were compared with the initial readings before transfer to calculate the change in strain. A trend line was then calculated for the end of the beam to the point where the change in strain became zero using a least squares regression. The 95 Percent Average Maximum Strain (95% AMS) method was used to calculate the strain profile for change in strain plateau. The point where the trend lines for the sloped portion of the curve and the plateaued portion of the curve intersect is the transfer length for the member.

Transfer lengths for the CSA cement concrete voided deck slab and the traditional Portland cement voided deck slab were compared up until three days after transfer. DEMEC measurements were unable to be read after three days because the manufacturer prepared the slab for transportation. Transfer length estimations via concrete surface strain and strand end-slip were taken for the Portland cement concrete slab in order to have an approximate comparison with the same design.

Figure 3.11 DEMEC Placement

Figure 3.12 Concrete Surface Strain Calipers

Strand end-slip measurements were also taken immediately before and after transfer using a micrometer with accuracy to 1/1000th of an inch. A paint marker was used to mark a reference point on the strands, and the micrometer was used to measure the distance from the end of the forms to the mark on the strands. Three initial measurements were taken immediately before transfer followed by three final measurements immediately after transfer. Equation 2.2 was used to calculate the transfer length from the end-slip measurements. End-slip measurements are often difficult to keep precise, thus the values for each measurement were taken as the average of the initial and final measurements. The end form setup is shown in Figure 3.13.

Figure 3.13 End Form Strand Setup

3.3.7.2 Vibrating Wire Gages

In addition to concrete surface strain measurements being taken from DEMECs, vibrating wire strain gages (VWSGs) were also cast into the voided deck slab. A series of eight total VWSGs were cast into the member and attached to the strands at both the top and bottom strands using zip ties, which can be seen in Figure 3.14. Four VWSGs were placed at midspan, with two strain gages on the top strands and two strain gages on the bottom strands. The remaining four strain gages were attached to top and bottom strands at quarter and three-quarter points along the length of the member.

The VWSGs had both strain and temperature sensors, and samples were taken once every 30 seconds for the lifetime of the beam before the final destructive tests. Prestress losses were estimated using the strain data from the VWSGs along with the laboratory mix replication data.

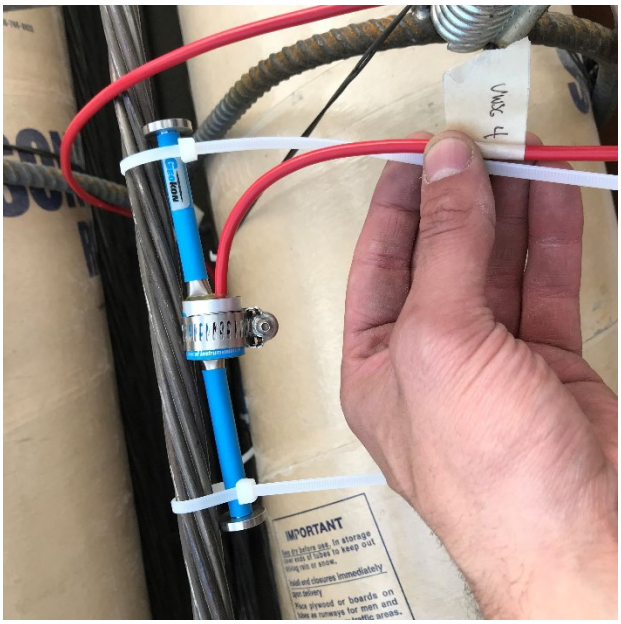

Figure 3. 14 VWSG Placement

3.3.7.3 Camber

Camber changes due to the eccentricity of the prestress force on the member cross-section. Camber was measured using an engineer's level and steel ruler accurate to one-tenth of a millimeter to calculate the change in elevation along the length of the member. The measurements taken from the engineer's level were compared with the expected camber given in the AASHTO and PCI Bridge Design provisions in Section 2.3. Both initial and long-term camber were measured, as time-dependent effects such as creep can lead to changes in camber over the lifespan of the bridge.

3.4 Full-Scale Beam Testing

The final phase of the material testing program was to test the full-scale prestressed voided deck slab. The 22-ft-long voided deck slab was designed by Olympus Precast in Bluffdale, Utah. The specifications for the rebar, prestressing strands, and cross-sectional dimensions can be found in Figures 3.15 and 3.16. The voided deck slab was stored on 4 x 4 wood dunnage placed underneath the lifting anchors four feet from either end of the beam. The full-scale beam testing consisted of a crack initiation test, a crack reopening test, and two shear tests, one at midspan and one near the end of the beam.

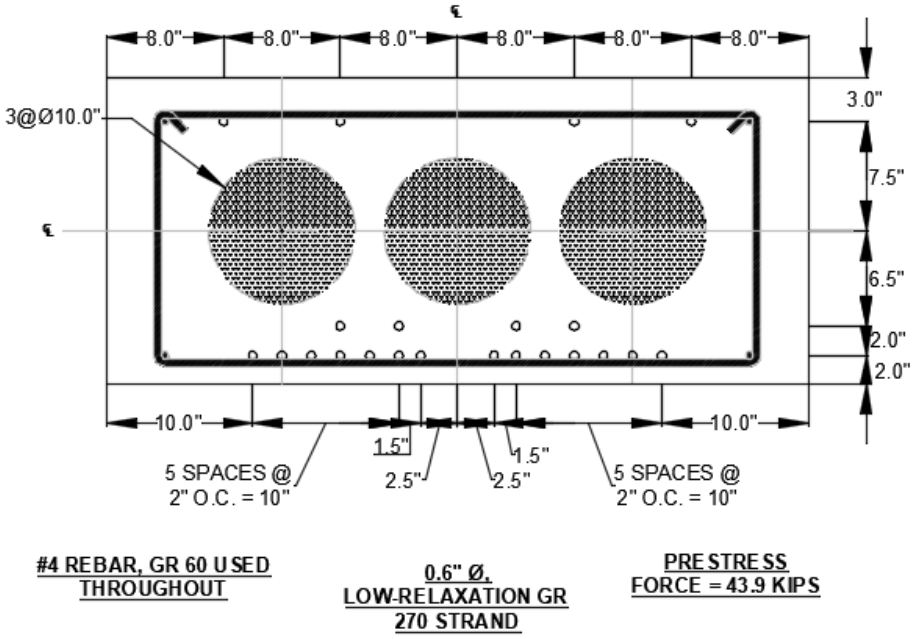

Figure 3.15 Voided Deck Slab Cross-Section

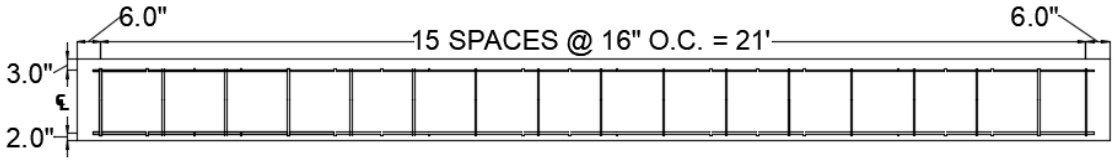

Figure 3.16 Voided Deck Slab Transverse Rebar Configuration

3.4.1 Crack Initiation Test Setup

The crack initiation test setup consisted of a single point load centered over the beam in order to induce cracking near the midspan of the member. The crack initiation test procedure consisted of incrementally loading the beam and measuring change in strain for each loading increment. Expected flexural cracking loads can be approximated assuming a modulus of rupture of $0.20\sqrt{f'_c}$, which corresponds to the lowest modulus of rupture specified for normal weight concrete as per AASHTO Article 5.4.2.6. Figure 3.17 shows the test setup for the crack initiation test.

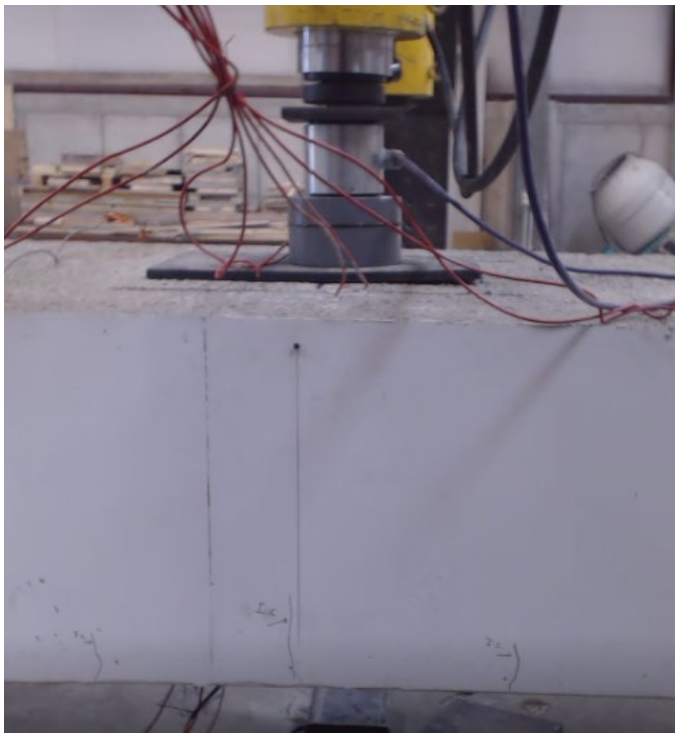

Figure 3.17 Crack Initiation Test Setup

3.4.2 Crack Reopening Test Setup

As discussed in Section 2.2.2, the crack reopening test is done in order to determine the load at which the initial crack reopens. The use of this information allows for an estimation of the effective prestress force in the girder. The test setup for the crack reopening test was the same as shown in Figure 3.17 for crack initiation tests except with new strain transducers, which spanned the crack formed in the crack initiation test. The strain gage was attached with 30-second epoxy. Load was applied as constantly as possible until the crack reopened. A real-time load vs. strain plot was used to determine the point of nonlinearity, which indicates the reopen of the initial crack. The initial crack was calculated to occur below the applied load. Four strain transducers were fixed to the beam across the crack, with the average strain in each strain transducer. Three cracks formed initially in the bottom of the beam, and the strain transducers spanned the middle crack, as seen in Figure 3.17, on the extreme fiber of the beam.

3.4.3 Midspan Test Setup

The voided deck slab was tested for development length after the member finished sustaining prestress losses, as monitored by the vibrating wire strain gages cast at the quarter and midpoints of the beam. Midspan testing in this context consisted of a single point load over the midspan of the beam, as in the crack initiation and reopening tests. Figure 3.17 shows the placement of the load for the development length test. The load was applied continuously and the beam was taken to failure. Crack initiation and crack reopening tests must be performed prior to the shear tests, as the shear test is a destructive test, whereas the crack initiation and crack reopening tests are only partially destructive tests. These crack initiation and reopening tests were carried out as described in Section 3.4.1 and Section 3.4.2.

3.4.4 Girder Shear Test Setup

One shear test was performed on the voided deck slab at a distance 1.25d from the face of the support. The test consisted of placing the end of the beam, if undamaged, on a steel bearing surface, and applying a load continuously until failure. Figure 3.18 shows the test setup for the shear tests.

Figure 3.18 Typical Girder Shear Test Setup

The shear tests were composed of a distributed point load over the width of the bridge girder at a distance $1.25d_v$ from the support (Pettigrew 2014). LVDTs were fixed to the exposed strands to measure strand end-slip. Wire potentiometers were placed on either side of the beam to measure deflection underneath the load. Two 300-kip hydraulic rams were used to apply the load over a 7 in. x 7 in. x 5/8 in. HSS beam filled with 5000 psi concrete to prevent buckling.

4. MATERIAL TESTING RESULTS

4.1 Material Testing Results

Experimental results for the material testing program are summarized in the following chapter. The data were collected and analyzed according to ASTM standards and according to methods described in the literature review in Chapter 2. All experimental methods are described in Chapter 3.

4.2 Concrete Mix Design

The concrete mix design is described in Section 3.2. The day of the concrete pour, test results did not follow the laboratory results for the mix design. After experimental testing and trial and error, the concrete mix was believed to have trace amounts of Portland cement in addition to the CSA cement in the magnitude of about 2.48% replacement by weight. Based on several trial and error laboratory batches, the most accurate concrete mix design to reflect the as-built member is summarized, per yard of concrete, in Table 4.1.

4.3 Day of Pour Concrete Testing

On the day of casting, the voided slab concrete testing was carried out as described in Chapter 3. The results for each test at Olympus Precast are described in the following section.

4.3.1 Compression

A series of 29 concrete cylinders were tested in compression on the day of the concrete pour, with cylinders also tested at three days, seven days, 14 days, 28 days, and the day of the full-scale beam testing. Figure 4.1 summarizes the results of the compressive strength development of the concrete poured at Olympus Precast on June 1, 2018.

Table 4.1 Actual Mix Proportions (quantity per yard)

CSA Mix Proportions	
682.64	lb CTS
17.36	lb PC
320	lb Water
1650	lb Coarse
1150	lb Fines
98	oz Advacast
52.5	oz Daravair
182	oz Recover

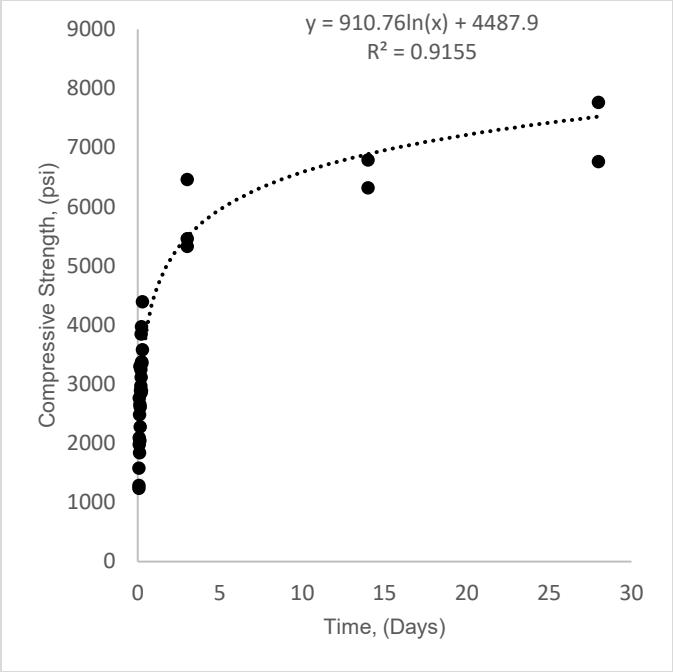

Figure 4.1 Olympus Concrete Compressive Strength Development

Compressive strength at the time of release was 4396 psi, taken at 6.75 hours after mixing began. The 28-day compressive strength of the concrete was 7264 psi +/- 707 psi.

4.3.2 Dynamic Elastic Modulus

Dynamic elastic modulus of the concrete was tested as described in Chapter 3. The results for dynamic elastic modulus of the concrete are summarized in Figure 4. 2.

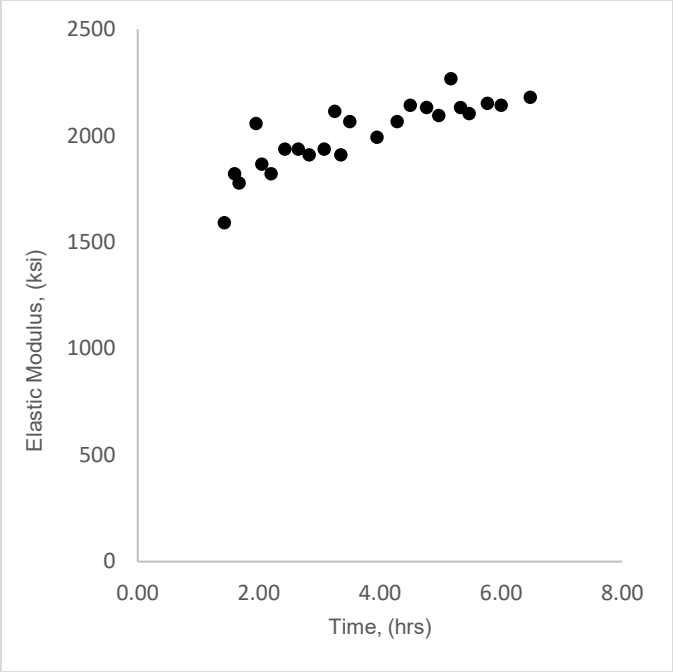

Figure 4.2 Dynamic Elastic Modulus Development

Dynamic elastic modulus at the time of release was 2181 ksi. Dynamic elastic modulus results were not available after the first day of testing for the Olympus concrete mix.

4.3.3 Set Time

Initial and final set for the Olympus concrete were 72 and 78 minutes, respectively.

4.4 Laboratory Mix Replication

The laboratory mix replication test results are summarized in the following sections. Compression, tension, dynamic elastic modulus, static elastic modulus, drying shrinkage, autogenous shrinkage, and creep tests were conducted in the laboratory as described in Section 3.3.1. Initial and final set times were 47 and 53 minutes, respectively. The shorter set times were due to the higher temperatures on the days the mixes were made.

4.4.1 Compressive Strength

Compression tests were carried out on the laboratory mix as described in Section 3.3. Compression tests were performed on cylinders at two hours, four hours, six hours, 24 hours, 14 days, and 28 days after mixing of the concrete began. Due to the limited volume of the concrete mixer, no tests were performed after six hours on the first day. All cylinders were stored in a temperature and humidity controlled room at Utah State University. Figure 4.3 summarizes the results of the compressive strength development of the laboratory mix.

The compressive strength at six hours for the laboratory mix was 3899 psi +/- 261 psi. The 28-day compressive strength of the laboratory mix was 6337 psi +/- 266 psi.

4.4.2 Tensile Strength

Tensile strength testing for the laboratory mix concrete was carried out as described in Section 3.3.1. The test results for the splitting tension tests had high variability during early age. Figure 4.4 summarizes the tensile strength results from the splitting tension tests.

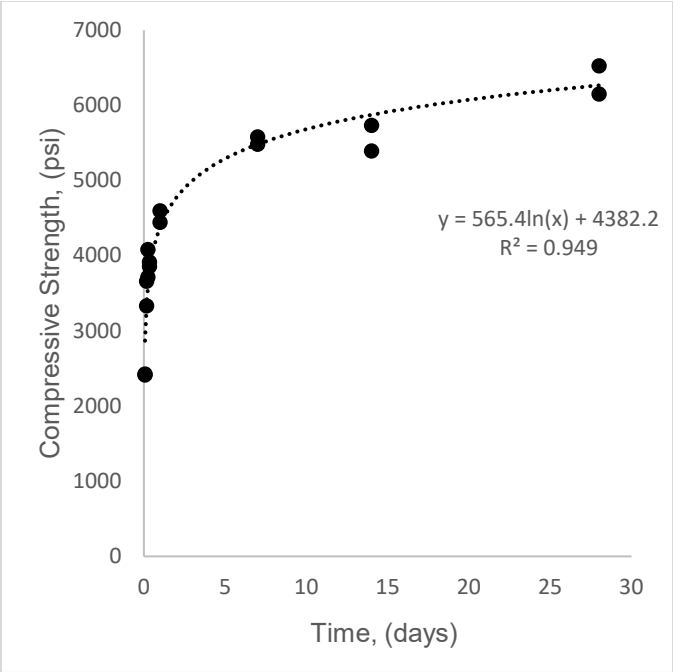

Figure 4.3 Laboratory Concrete Compressive Strength Development

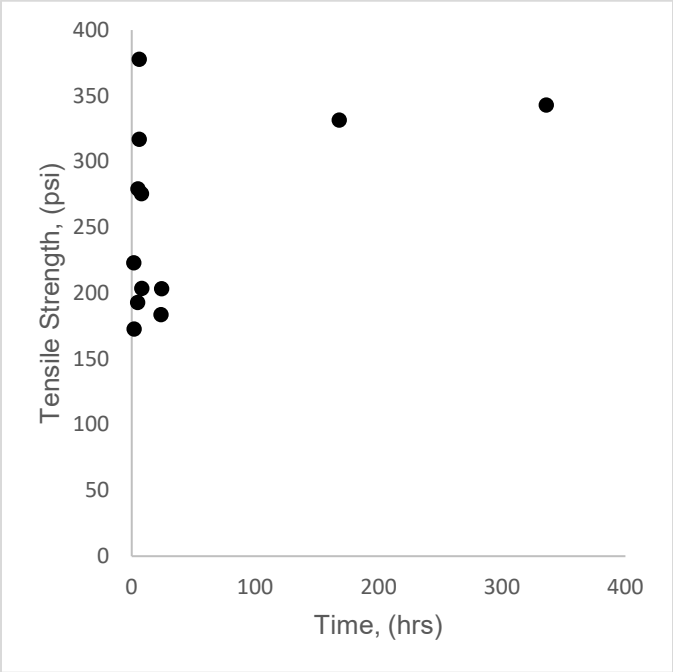

Figure 4.4 Tensile Strength Development

4.4.3 Dynamic Elastic Modulus

Dynamic elastic modulus testing was done using an NDT James Instruments Emodumeter, as seen in Figure 3.2. The emodumeter relates the frequency of resonance of the cylinders and uses an equation to relate the frequency to the dynamic elastic modulus. The development of dynamic modulus is summarized in Figure 4.5.

4.4.4 Static Elastic Modulus

Static elastic modulus was measured as described in Section 3.3.3.3. Static modulus was calculated from the slope of the stress-strain curve from loading and unloading the cylinder in the elastic region. Static elastic modulus development is summarized in Figure 4.6.

4.4.5 Creep

Creep strain was measured as described in Section 3.3.3.5. Strain from creep was then calculated as the change in length divided by the gage length. Strain was then zeroed by considering the initial measurement before load was applied to be zero strain. Creep strain was measured along three different gage lengths per cylinder and then averaged on a cylinder-by-cylinder basis. The results of the creep strain measurements, as well as the average for all cylinders, are summarized in Figure 4.7.

4.4.6 Drying Shrinkage Strain

Strain due to drying shrinkage was measured using the frame as shown in Figure 3.16. Strain is calculated as the change in length divided by the initial length of each specimen. Specimen dimensions were taken multiple times, and included the pins used to fix the specimen into the frame. Drying shrinkage strain results are summarized in Figure 4.8.

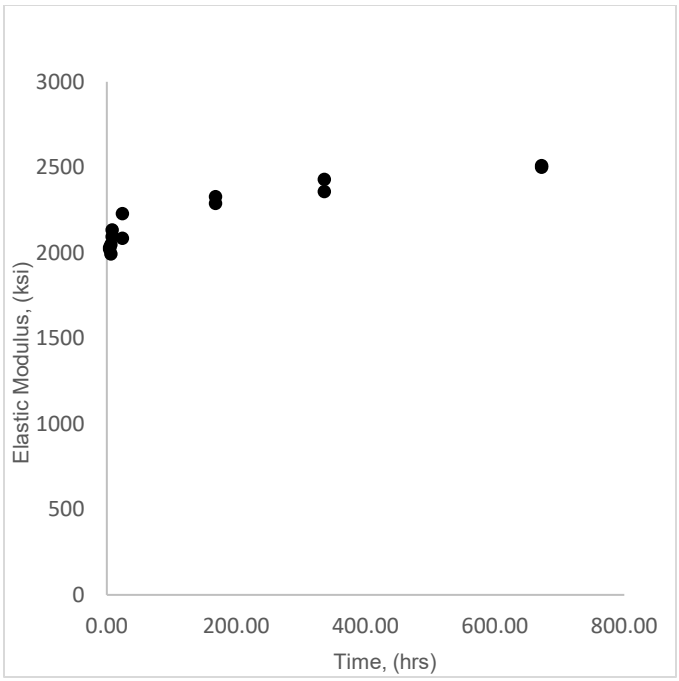

Figure 4.5 Dynamic Elastic Modulus Development

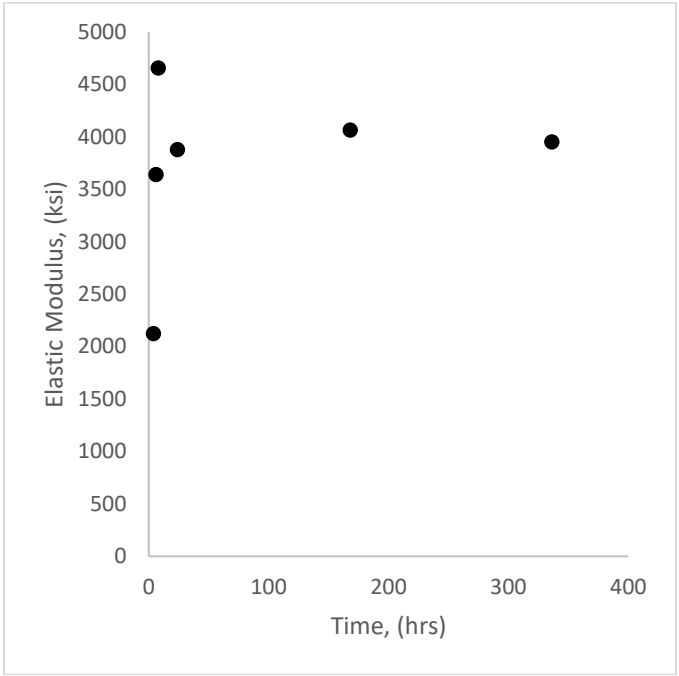

Figure 4.6 Static Elastic Modulus Development

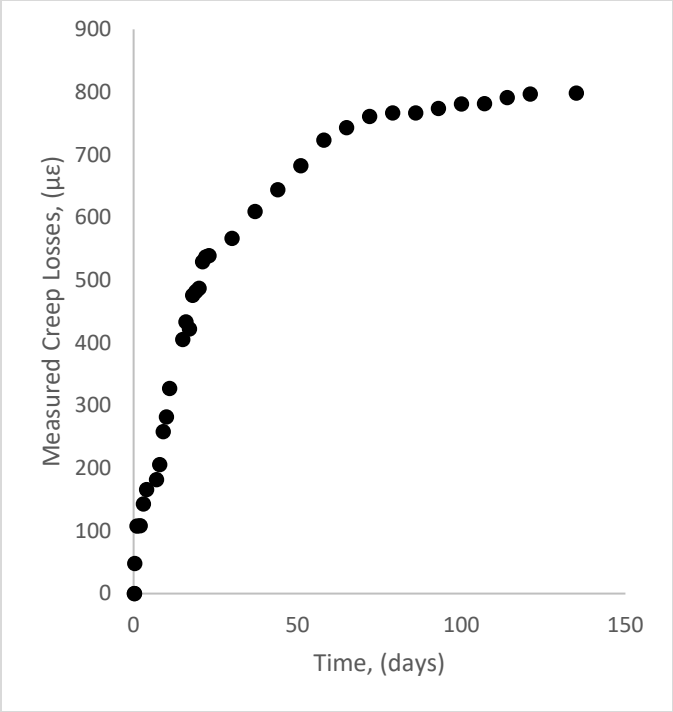

Figure 4.7 Creep Strain vs. Time

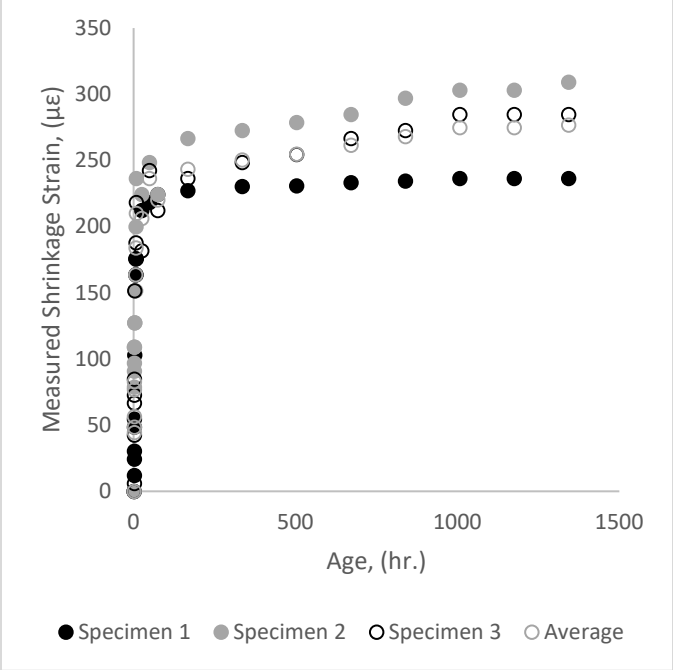

Figure 4.8 Drying Shrinkage Strain vs. Time

4.4.7 Autogenous Shrinkage Strain

Strain due to autogenous shrinkage was measured using the autogenous shrinkage frame as seen in Figure 3.6. Strain is calculated by taking the change in length divided by the gage length of the specimen. Specimen gage lengths were measured three times in different locations and averaged. The strain due to autogenous shrinkage is given in Figure 4.9

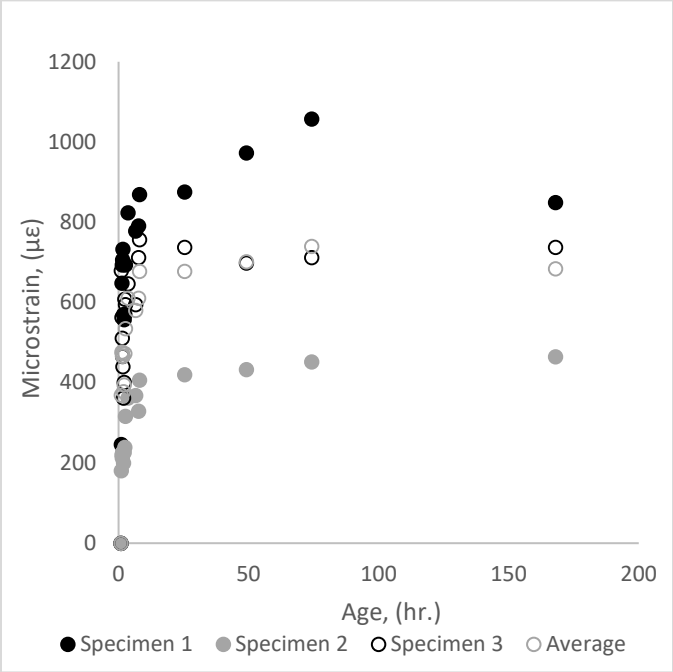

Figure 4.9 Autogenous Shrinkage Strain vs. Time

4.4.8 Total Shrinkage

Total shrinkage was estimated by adding the measured material testing results at each time step and plotting the sum of the results against time. Total shrinkage strain vs. time is summarized in Figure 4.10.

4.5 Transfer Length

Transfer length was measured as described in Section 3.3.4.1 using DEMEC strain gages. Figure 4.11a and Figure 4.11b show transfer lengths at various ages of the concrete for the live and dead ends of the beam, respectively. Transfer lengths were calculated using the 95% AMS Method as described in Section 3.3.4.1 and shown in Figure 4.12a and Figure 4.12b for both the dead and live ends of the beam, with AASHTO specified values of $50d_b$ and $60d_b$.

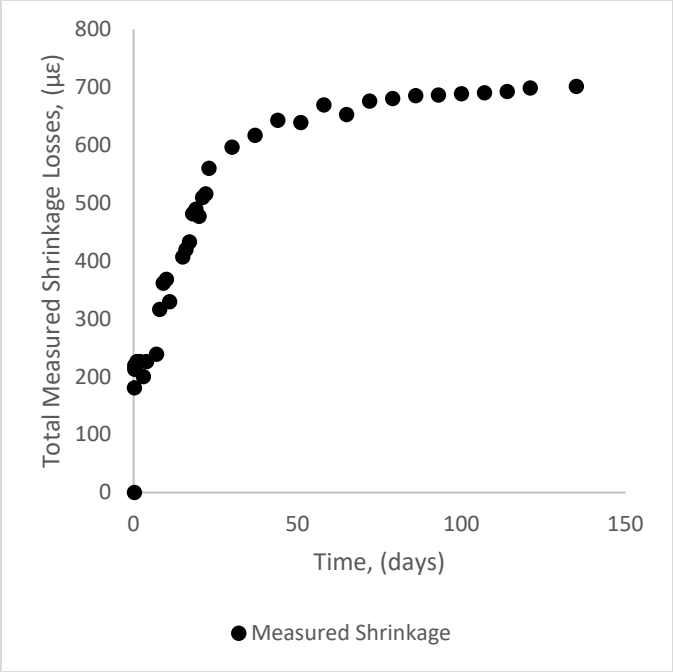

Figure 4.10 Total Shrinkage Strain vs. Time

Transfer length values are only available for the first 14 days after casting because too many DEMEC strain gages detached on each end of the beam to calculate the transfer length. Transfer length for a traditional Portland cement concrete voided slab of the same cross-section and design concrete strength was measured three days after transfer as a way to compare the two materials. Figure 4.5.3 shows the DEMEC measurements and 95% AMS offset. The measured transfer length for the Portland cement concrete was measured as 19.9 inches at three days after casting.

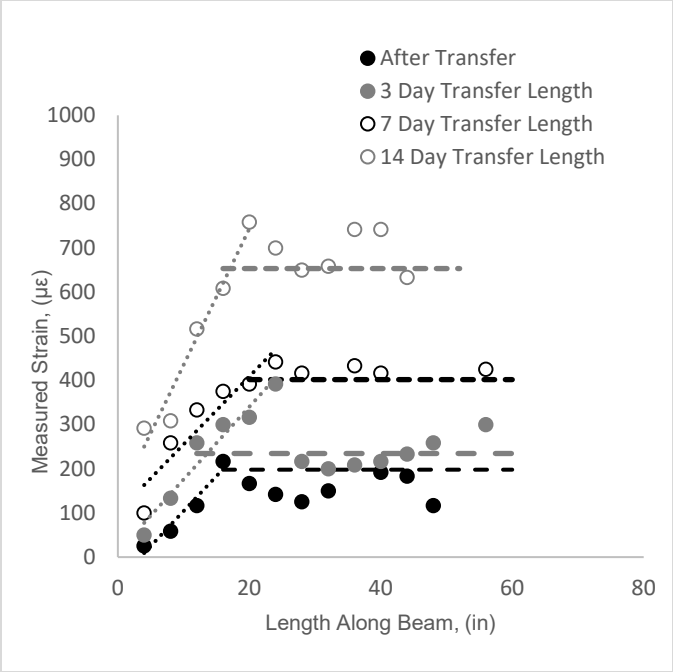

Figure 4.11a Dead End Transfer Length

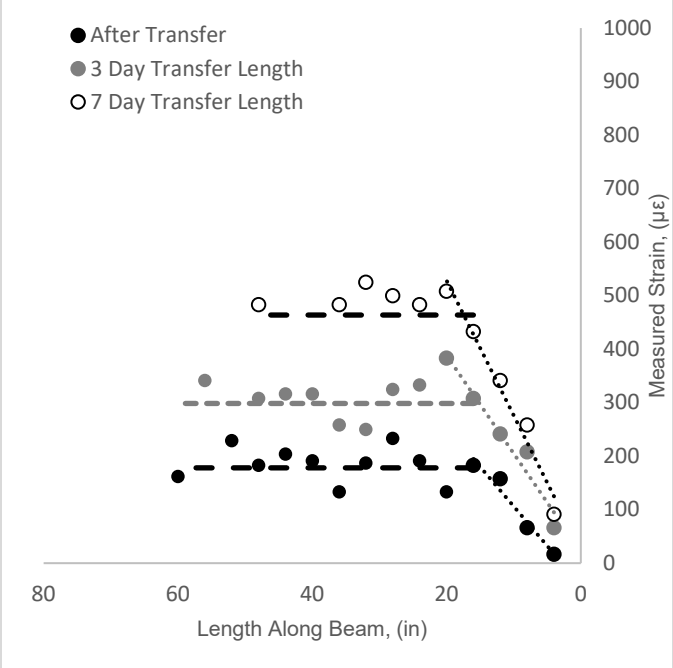

Figure 4.11b Live End Transfer Length

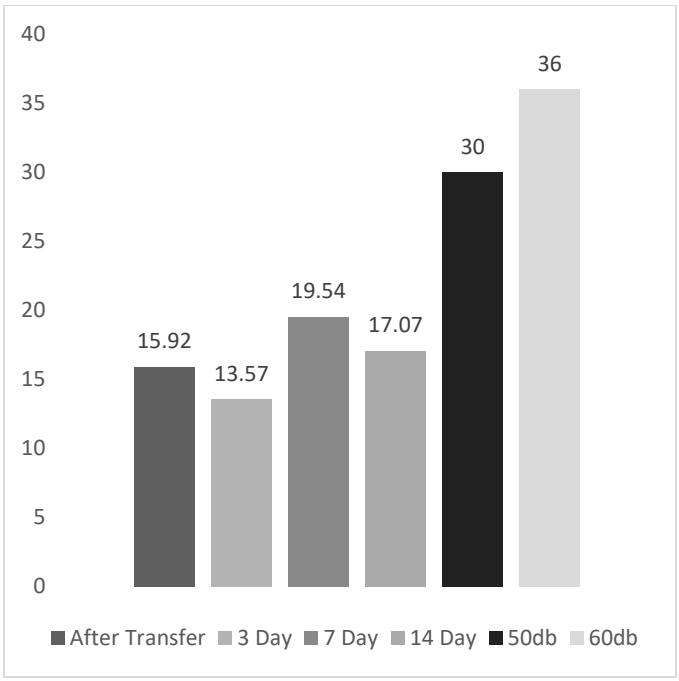

Figure 4.12a Dead End Transfer Length Values

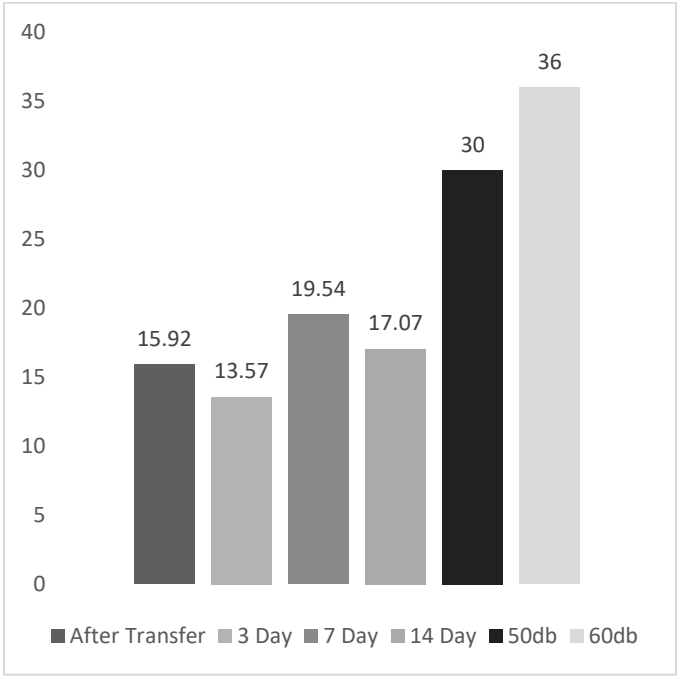

Figure 4.12b Live End Transfer Length Values

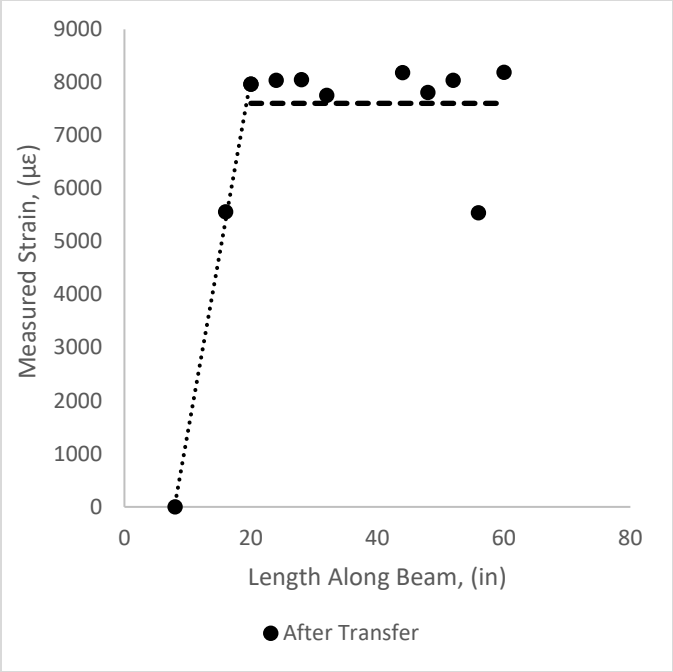

Figure 4.13 Portland Cement Concrete Transfer Length

Transfer length was also approximated using strand end-slip measurements immediately before and after transfer. Strand end-slip values are summarized in Table 4.2. Using raw slip measurements and Equation 2.2, strand end-slip was used to approximate transfer length values at four different strands on each end of the beam. Strand end-slip is a less reliable and highly variable measurement, as seen in the high standard deviation. Figure 4.12 summarizes the strand end-slip transfer length calculations for the Portland cement concrete beam cast in-line with the CSA beam.

Table 4.2 Strand End-slip Transfer Length for CSA Beam

E_{ps}, (ksi)	A_{ps}, (in^2)	F_{ps}, (kip)	f_{ps}, (ksi)	α	F_{ps}, (ksi)	
28500	0.219	43.9	200.46	2	270	Low relaxation

East End		End-slip	Transfer Length	West End		End-slip	Transfer Length
Before	After			Before	After		
1.0405	0.9620	0.0785	22.32	0.9555	0.8895	0.0660	18.77
1.0320	0.9450	0.0870	24.74	0.9035	0.8045	0.0990	28.15
1.0065	0.8445	0.1620	46.06	1.0925	0.9530	0.1395	39.67
1.0115	0.9345	0.0770	21.90	0.9595	0.8830	0.0765	21.75
						Average	27.08
						Std. Dev	9.26

Table 4.3 Strand End-slip for PC Beam

West End		End-slip	Transfer Length
Before	After		
0.9085	0.8260	0.0825	23.46
0.9095	0.7160	0.1935	55.02
0.9180	0.7840	0.1340	38.10
0.9765	0.7055	0.2710	77.06
		Average	48.41
		Std. Dev	23.05

5. PRESTRESS LOSSES

5.1 Experimental Results

Prestress losses on the voided deck slab were monitored both initially and long term with the use of laboratory concrete mix testing, vibrating wire strain gages embedded in the concrete, and a crack reopening test at the midspan of the voided deck slab.

5.2 Creep Losses

Measured creep on the concrete cylinders of the final laboratory mixture is compared to AASHTO predicted creep values in Figure 5.2.1. AASHTO predicted creep values were taken at a constant time step to form a curve that captures the full creep behavior of concrete. Creep of concrete is known to increase camber deflections in prestressed concrete and the amount of prestress losses experienced by the member.

Creep strain can be predicted for traditional Portland cement concrete using AASHTO Equation 5.9.5.4.2b-1 to find the loss due to creep and dividing by the elastic modulus at the time in question. AASHTO predicted creep was compared to the experimental results shown in Figure 5.1.

Based on the laboratory mix creep tests, the AASHTO equation for creep strain is very well suited for creep of CSA cement concrete under laboratory conditions and 50% humidity. At early loading times (up to about 28 days), prediction is nearly identical with measured strains dropping off significantly after 28 days and the prediction equation overestimating ultimate creep. Long-term creep strains may be overestimated by the AASHTO equation based on these results, but additional study would be required.

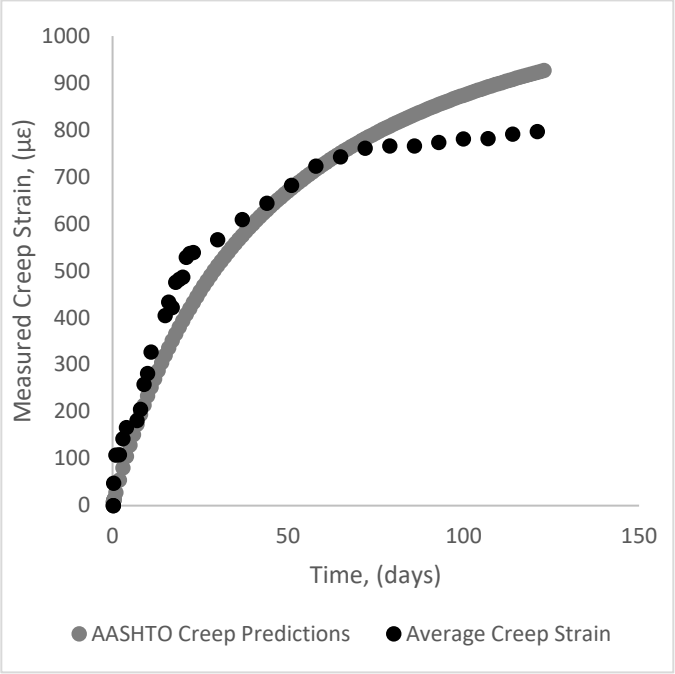

Figure 5.1 Comparing Measured to AASHTO Predicted Creep Strain

5.3 Total Shrinkage Losses

Total shrinkage losses were found by combining shrinkage from autogenous and drying shrinkage. While the AASHTO prediction is designed to consider drying shrinkage only, due to the large autogenous shrinkage in CSA cement, autogenous shrinkage may be significant enough to consider. AASHTO predicted shrinkage strain was calculated using AASHTO Equation 5.4.2.3.3-1 and compared to the total shrinkage strain in Figure 5.2.

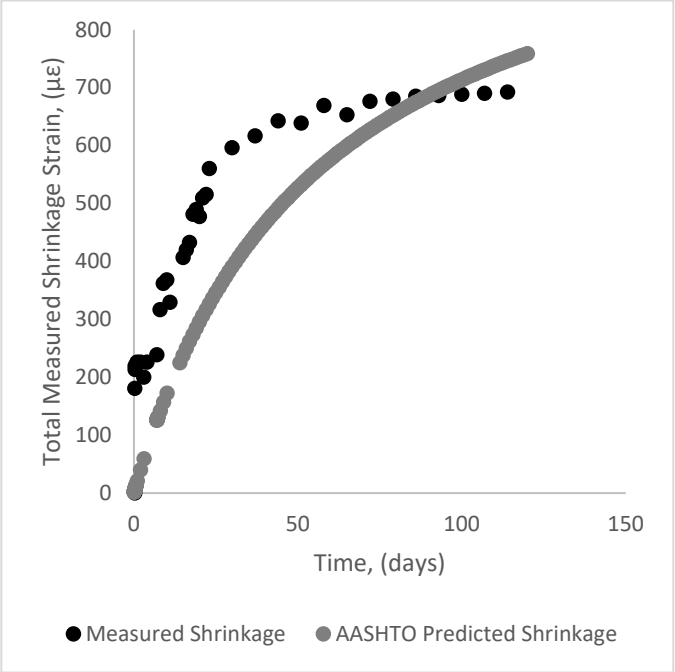

Figure 5.2 Total Shrinkage Strain vs. AASHTO Shrinkage Strain

The long-term shrinkage strain is overestimated for CSA cement concrete by AASTHO, but short-term shrinkage is underestimated. The major reason for the underestimation in the early age of the concrete is that autogenous shrinkage is measured without coarse aggregates. The coarse aggregates in a concrete are not subject to shrinkage during curing as the paste in the concrete is, and they actually provide shrinkage restraint. Therefore, autogenous shrinkage strain, as measured, is not necessarily appropriate to include in the calculation of shrinkage losses. A more appropriate measure for this purpose would be to modify the autogenous shrinkage specimen such that it can accommodate large aggregate.

5.4 Total Concrete Losses from Material Testing

Total concrete strains from the lab mixes were found by adding the strains from creep and shrinkage tests. Total prestress losses are summarized in Figure 5.3 and compared with the codified values from AASHTO. It should be noted that the lab mix data do not include elastic shortening. The AASHTO values for prestress loss were calculated assuming the same 50% humidity at which the material testing was performed.

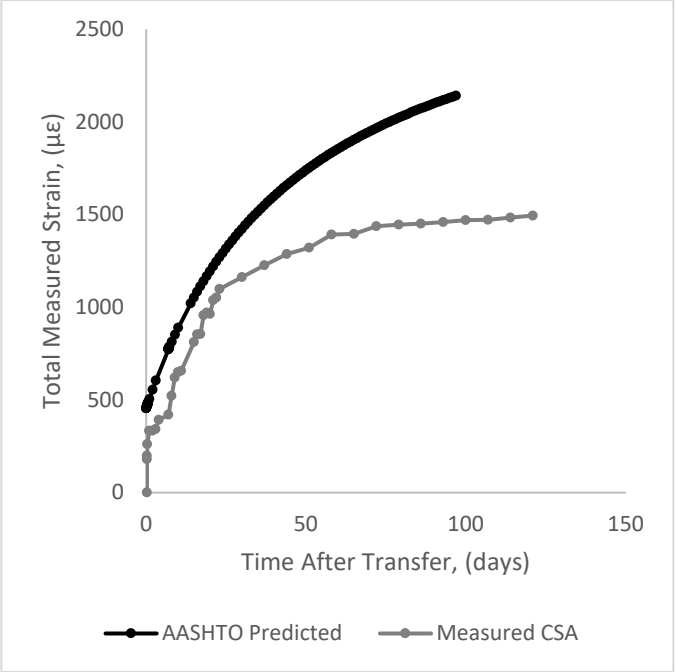

Figure 5.3 Total Strain from Lab Mixes

5.5 Concrete Time-dependent Strains Conclusions

AASHTO predicted losses for shrinkage at 14.9 ksi were below the measured ultimate shrinkage strain of 0.00693. This discrepancy may be because autogenous shrinkage is measured using a mortar instead of concrete (Quezada et al. 2018). A mortar has no coarse aggregates, which would restrain the concrete from shrinking. Without autogenous shrinkage added into the measured values, the measured ultimate shrinkage strain would be 0.00238.

AASHTO predicted losses for creep were very similar to the values measured from creep tests. Overall losses seemed to approach similar values, but the AASHTO equation for creep loss underestimated creep strain during the life of the member, with the ultimate predicted strain remaining above the measured ultimate creep strain of 0.000692. The AASHTO predicted ultimate creep strain was 0.000774.

5.6 VWSG Long-Term Losses

Vibrating wire strain gages were embedded in the concrete and measured temperature and strain over the life of the voided deck slab. Change in strain was corrected for temperature using the manufacturer's recommendations. VWSG data are summarized in Figure 5.4 to 5.16. Each VWSG had two plots, the first consisting of strain before transfer, and the second consisting of strain after transfer. VWSG 1 did not work and subsequently is not included in the data. VWSG 3 did not have intelligible data before transfer but began working after transfer; therefore, only the data from after transfer are included below. VWSG 5 had error readings before the concrete was poured but began working shortly afterward. Positive values indicate a tensile strain, and negative values indicate a compressive strain.

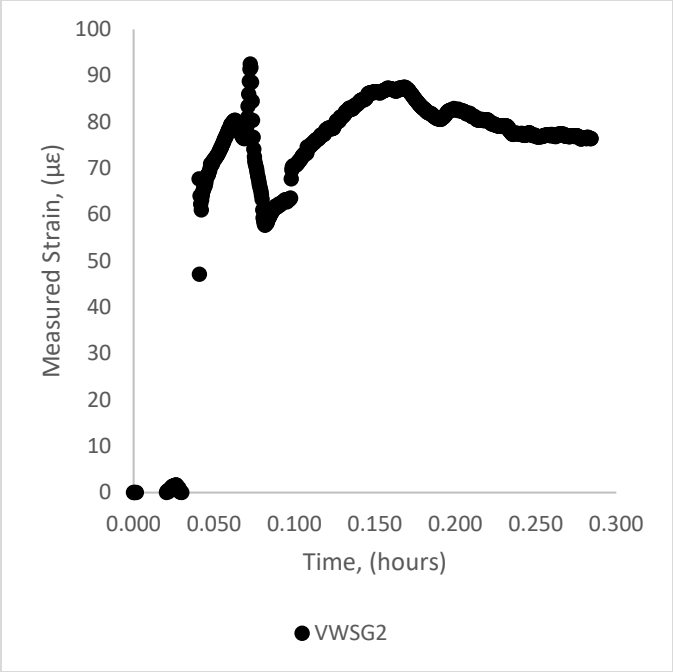

Figure 5.4 VWSG 2 Before Transfer

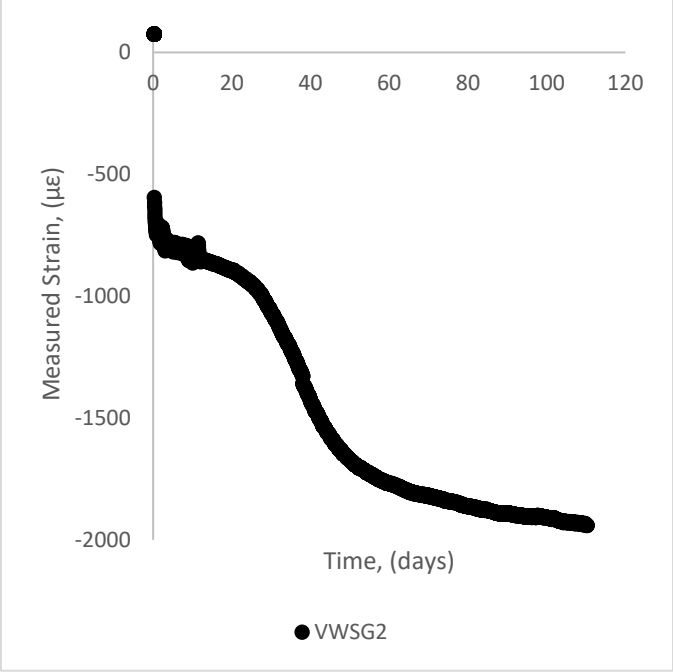

Figure 5.5 VWSG 2 After Transfer

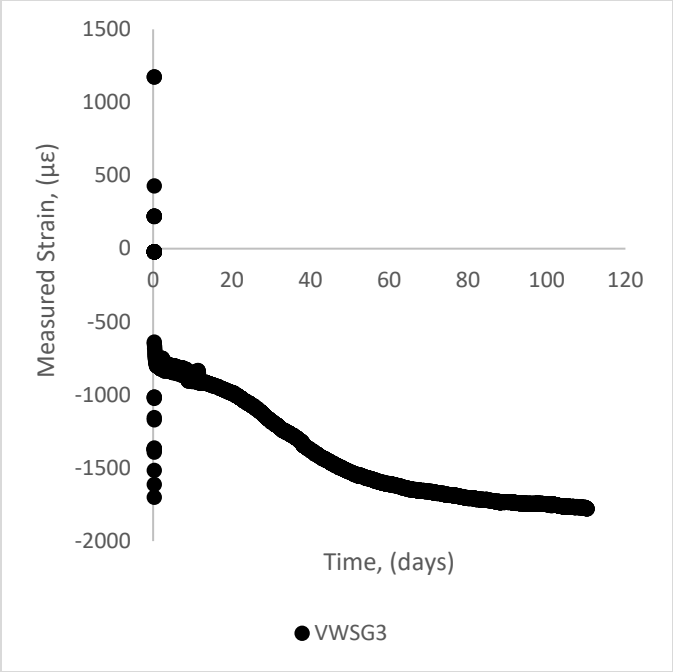

Figure 5.6 VWSG 3 After Transfer

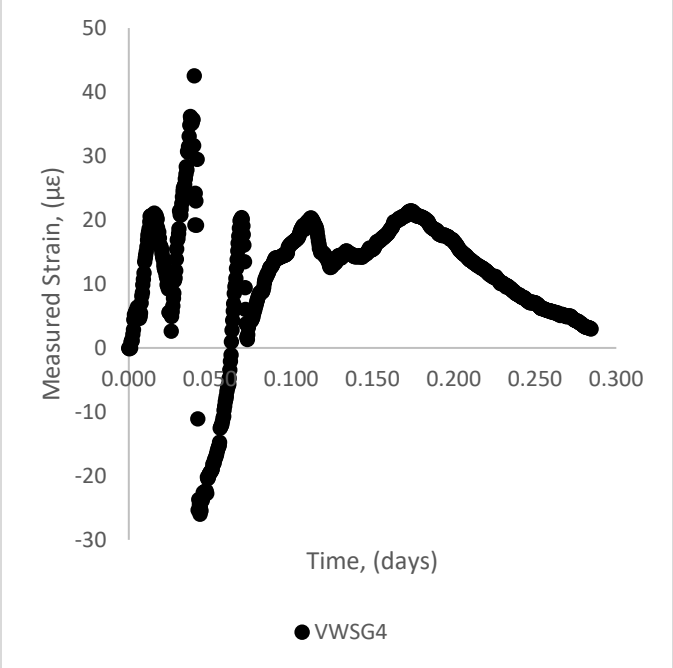

Figure 5.7 VWSG 4 Before Transfer

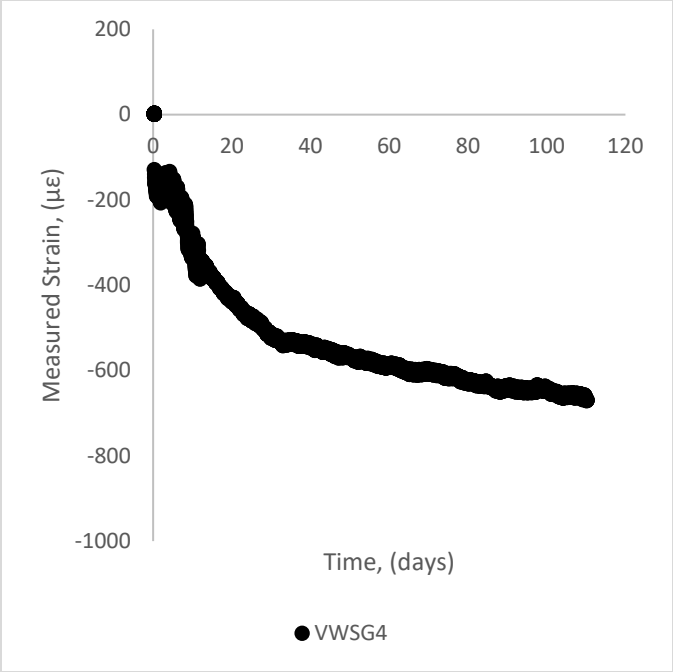

Figure 5.8 VWSG 4 After Transfer

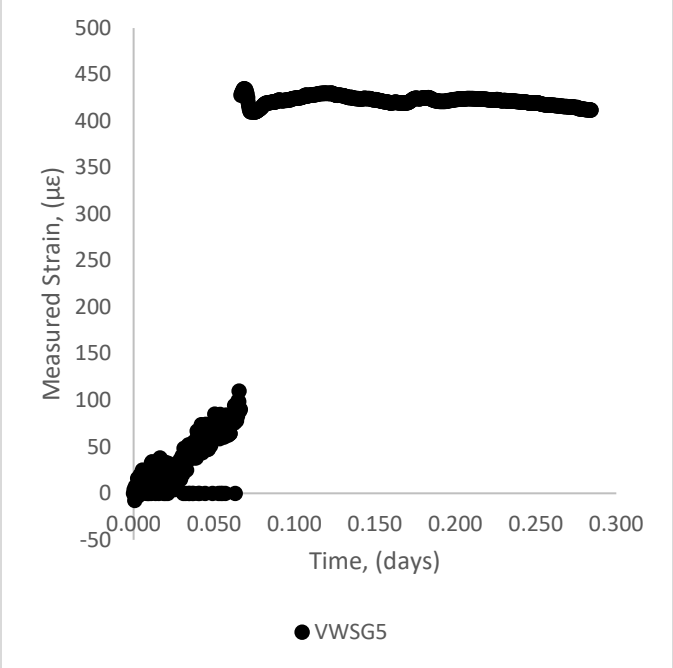

Figure 5.9 VWSG 5 Before Transfer

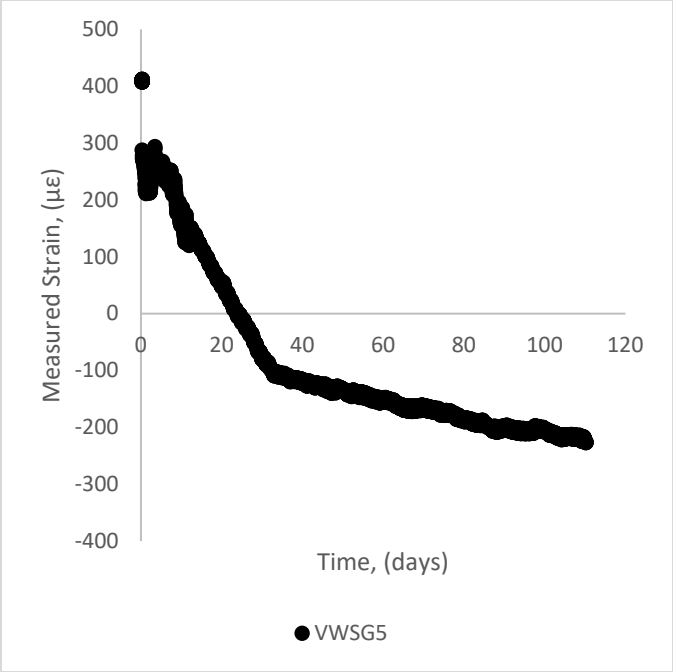

Figure 5.10 VWSG 5 After Transfer

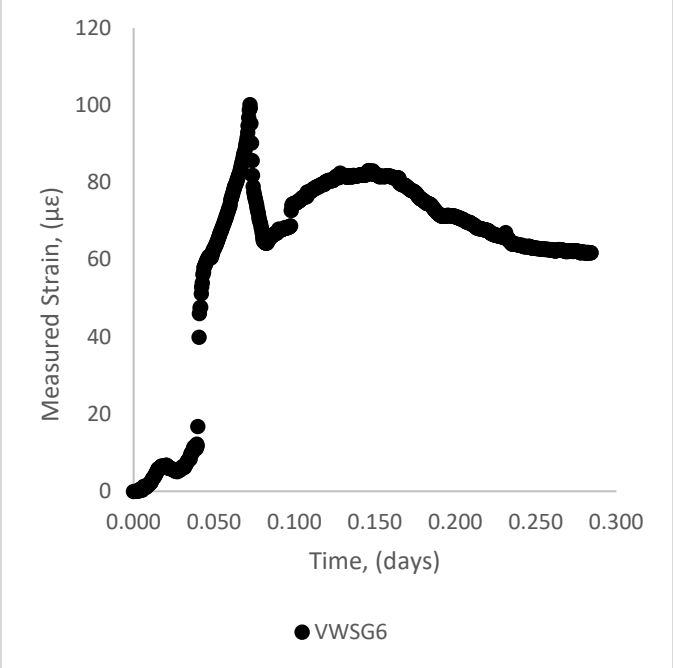

Figure 5.11 VWSG 6 Before Transfer

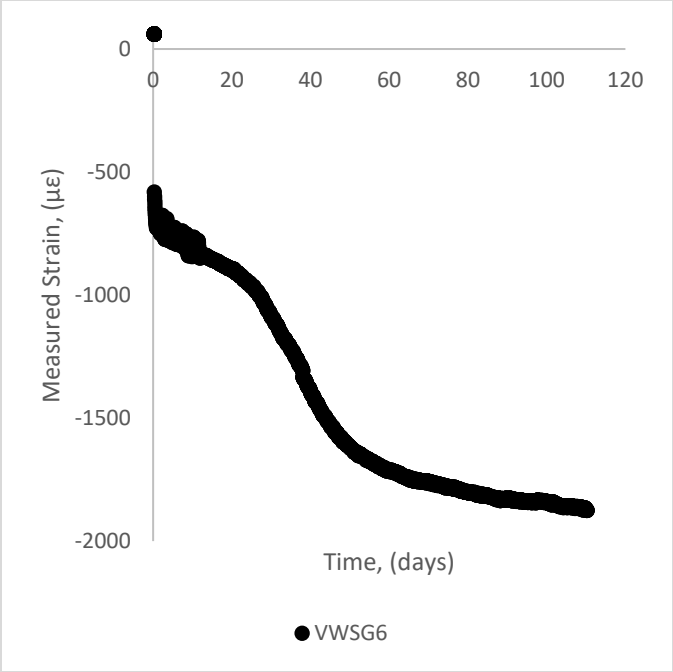

Figure 5.12 VWSG 6 After Transfer

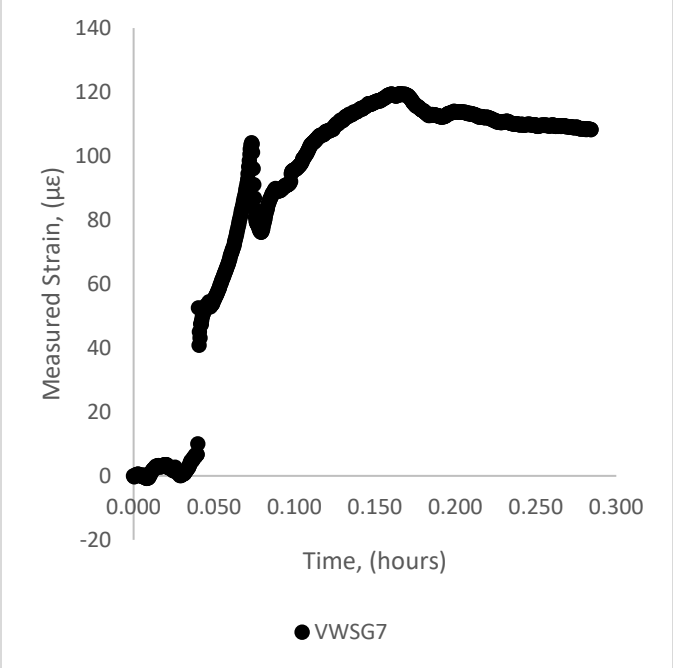

Figure 5.13 VWSG 7 Before Transfer

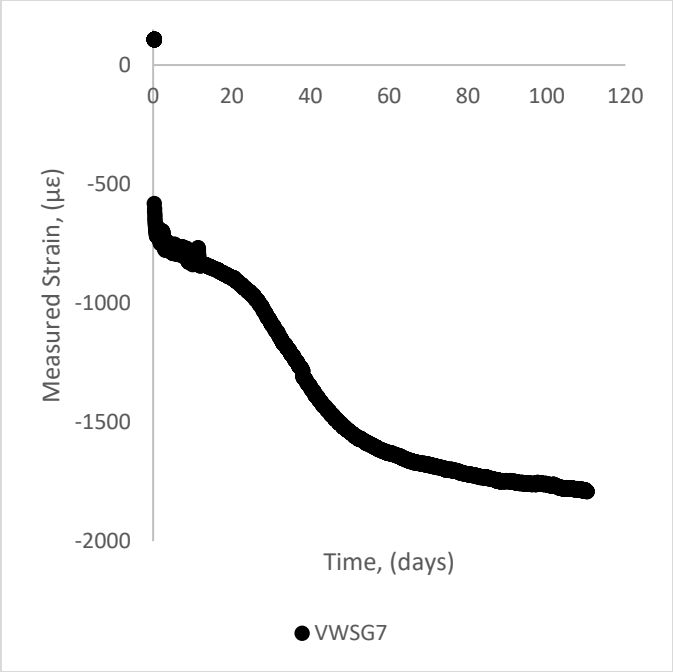

Figure 5.14 VWSG 7 After Transfer

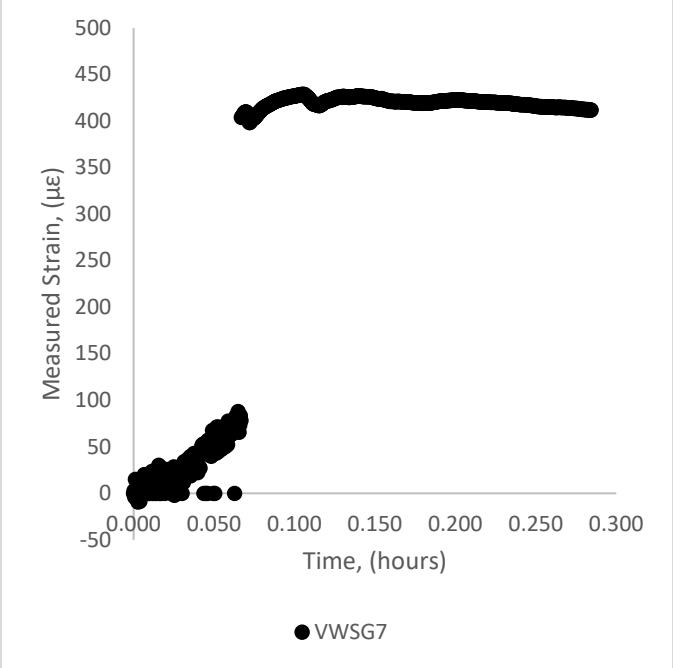

Figure 5.15 VWSG 8 Before Transfer

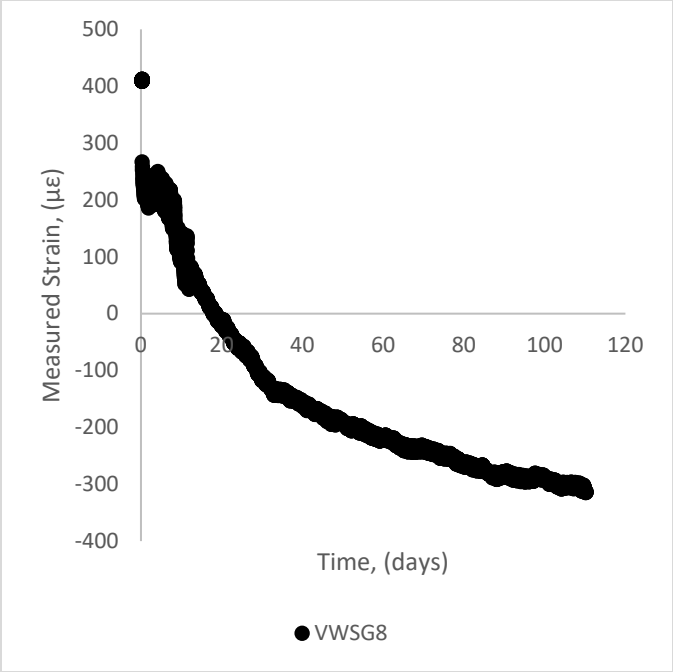

Figure 5.16 VWSG 8 After Transfer

The VWSG data show prestress losses over time, which can also be predicted using AASHTO Equation 5.9.5.1-1. Locations of the VWSGs in the voided deck slab are tabulated in Table 5.1. Only bottom strand VWSGs were considered in the comparison with the AASHTO equations. The comparison of AASHTO predicted prestress losses and as measured losses in the VWSGs is summarized in Figure 5.17. Prestress losses are considered positive in AASHTO, so the absolute value of the VWSG data was taken in the comparison. AASHTO predicted values of prestress losses were calculated assuming a humidity of 20% to match the conditions at casting and storage.

5.7 VWSG Prestress Loss Conclusions

AASHTO prestress loss predictions overestimated losses measured in the VWSGs, but appeared to approach the same value of ultimate prestress loss at the time of testing. The VWSG losses in the voided deck slab were amplified by supporting the voided deck slab on dunnage underneath the lifting anchors instead of at the ends of the beam. There was a rapid gain in the prestress losses beginning about 20 days after transfer, which coincides with transportation from Bluffdale to Logan. There was likely a restraint release due to movement from the dunnage, causing the change in the loss curve.

Table 5.1 VWSG Locations

VWSG	Location Along Length	Strand	Location Along Width
1	0.5L	Top	South
2	0.5L	Bottom	South
3	0.25L	Bottom	SouthEast
4	0.25L	Top	SouthEast
5	0.5L	Top	North
6	0.5L	Bottom	North
7	0.25L	Bottom	SouthWest
8	0.25L	Top	SouthWest

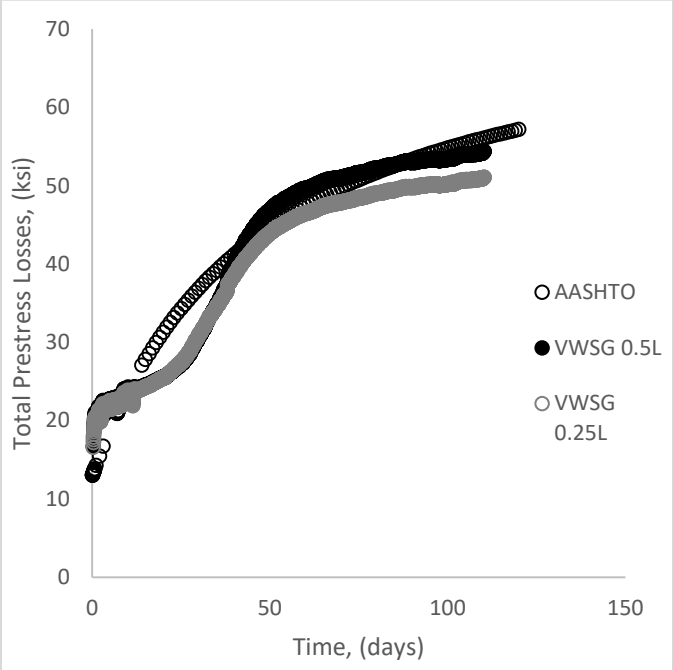

Figure 5.17 Average VWSG Prestress Loss vs. AASHTO Predicted

5.8 Camber

Camber measurements were taken as described in Section 3.3.4.2 using an engineer's level and ruler accurate to a tenth of a millimeter. Camber measurements were taken before transfer for the baseline, immediately after transfer, 14 and 28 days after casting, and the day of testing. Camber development is plotted in Figure 5.18.

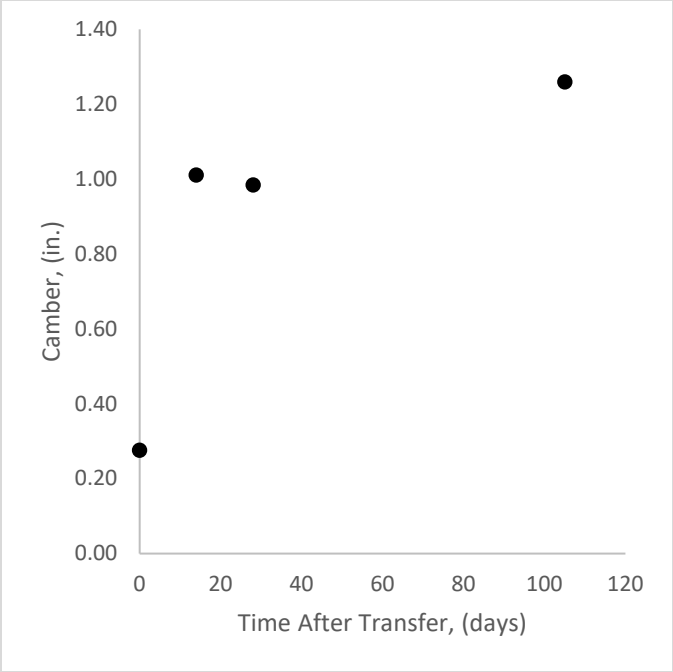

Figure 5.18 Camber Development

Camber development was exaggerated due to the boundary conditions during loading. The voided slab was placed on dunnage underneath the lifting anchors, located about 4 ft. from the ends of the beam. Initial camber can be calculated using basic mechanics for an initial camber deflection of 0.400 in. upward and 0.972 in. upward for long-term camber. Initial camber as measured was 0.280 in. upward, and final camber as measured was 1.260 in.

5.9 Camber Conclusions

The short cantilever at either end of the beam caused a negative bending moment, thus amplifying the deflection due to both self-weight and the eccentric loading from the prestressing strands. Supporting the beam underneath the lifting anchors, as opposed to the ends of the beam, definitely caused the increase in measured camber over time. Predicted values of initial and long-term camber using basic mechanics and long-term PCI multipliers were 0.40 in. and 0.972 in, respectively. The initial camber prediction overestimated camber by 0.12 in., and long-term camber was underestimated by 0.288 in.

5.10 Crack Initiation

Crack initiation tests were carried out as described in Section 3.4.1. Load was applied monotonically at a constant rate, held at a constant load to check for cracks around the cracking prediction, and increased until cracking occurred. Crack initiation test load vs. deflection results are summarized in Figure 5.19. Load was measured using a 400 kip load cell and deflection was measured using a wire potentiometer with a 20-in. range.

Maximum load for the crack initiation test as tested was 159.79 kips, and the corresponding deflection of the beam directly beneath the load was 0.0079 in. Along with vertical deflections, strand end-slip was also measured at either end of the beam using

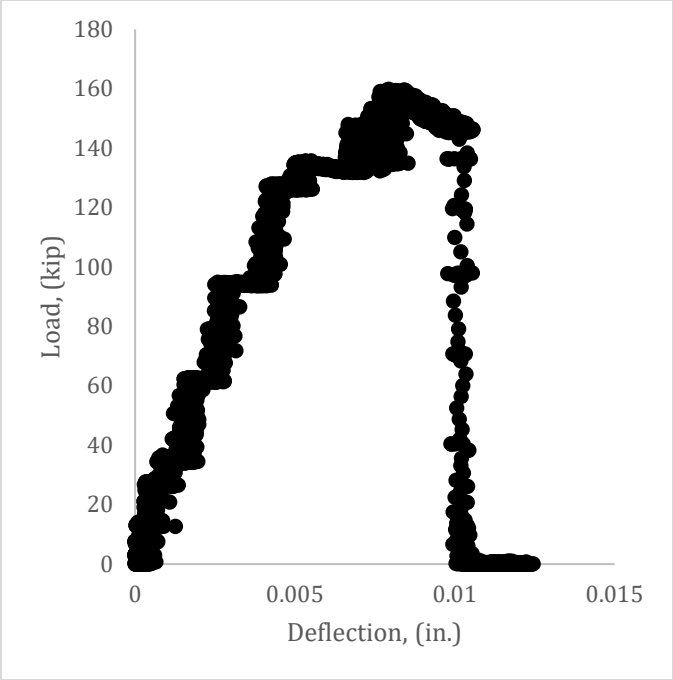

Figure 5.19 Crack Initiation Load vs. Deflection

LVDTs fixed to the strands using hose clamps, as seen in Figure 5.20. A steel angle was also attached to the end of the beam with epoxy to ensure a smooth surface for the LVDT to measure slip. No strand end-slip occurred during the crack initiation testing. Figure 5.21 shows the cracks formed in the voided deck slab from crack initiation test.

Figure 5.20 Typical LVDT Placement

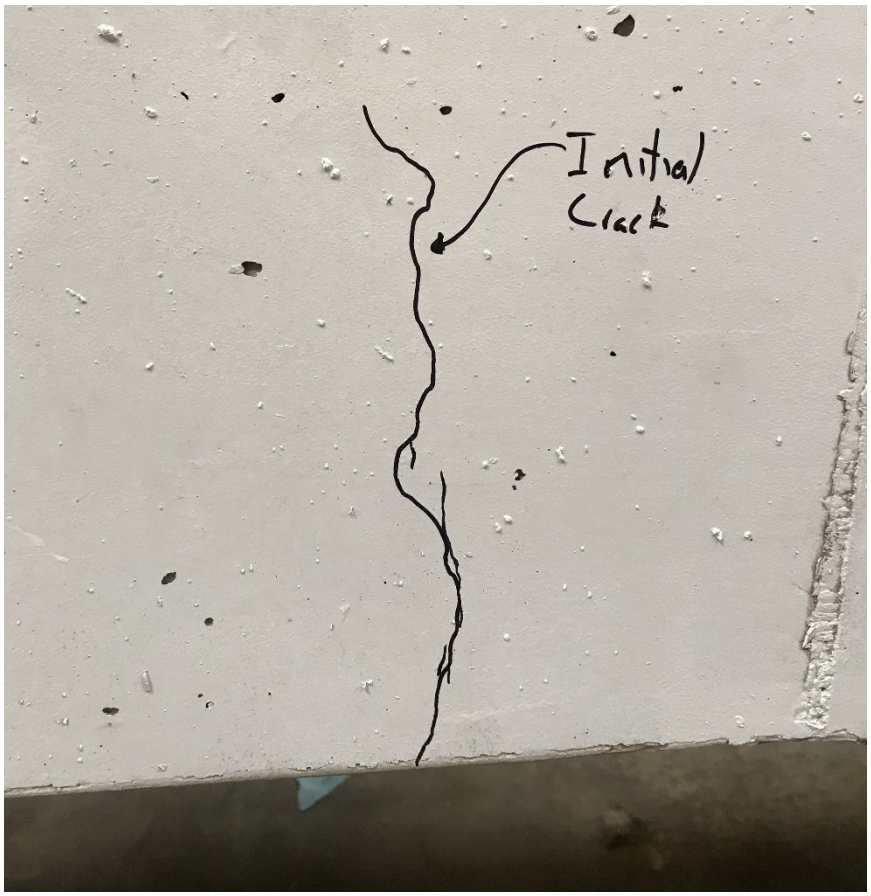

Figure 5.21 Crack Initiation Cracks in the Voided Deck Slab

5.11 Crack Reopening

Crack reopening tests were carried out as described in Section 3.4.2. Load was applied until the load verses deflection became nonlinear. In order to ensure the load applied was large enough to reopen the cracks in the beam, the load applied was greater than the load applied in the crack initiation test. Crack Reopening load verses strain across the crack is summarized in Figure 5.22. Strand end-slip was also monitored in this test, but the plates fastened to the end of the beam with epoxy detached, so the LVDT data were not usable.

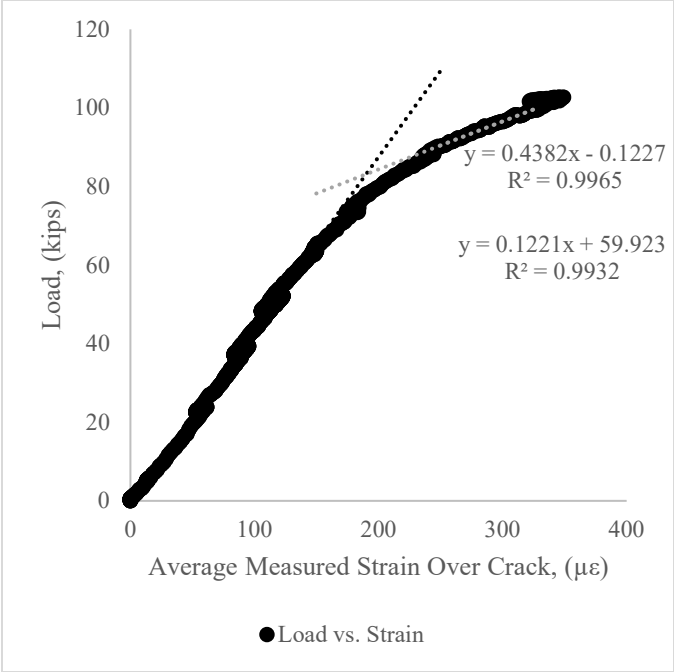

Figure 5.22 Crack Reopening Load vs. Strain along Initial Crack

Using the crack reopening data for load and strain, a least squared regression was performed to fit a line to the two distinct portions of the graph. The point at which these lines intersect is considered the crack reopen load. The measured crack reopening load for the voided deck slab was 83.12 kips, with a strain reading of 190 μin./in. This crack reopening load can be used to estimate the effective prestress in the voided deck slab using mechanics and Equation 5.1.

$$f_{pe} = \frac{\frac{M_{tot} y_b}{I_n}}{\frac{A_p}{A_n} + \frac{A_p e_n y_b}{I_n}} \tag{5.1}$$

Using Equation 5.1, the effective prestress from the crack reopening test was calculated to be 138.2 ksi. The total moment in Equation 5.1 includes the self-weight and the applied cracking load of 83.12 kips.

5.12 Crack Reopening Test Conclusions

Crack reopening test results lead to a low effective prestress in the bridge girder. The AASHTO predicted effective prestress for the bridge girder at the time of the test using AASHTO Equation 5.9.5.3-1 for time-dependent losses was calculated to be 139.08 ksi. AASHTO appears to be able to accurately predict prestress losses as measured from the crack reopening test for CSA cement concrete.

5.13 Prestress Losses Conclusions

Prestress losses were measured using many different methods, including material testing, VWSGs cast into the concrete, camber development, and a crack reopening test. The total prestress loss in the beam as calculated by the material testing, VWSG data, and the AASHTO predicted equations are given in Figure 5.23.

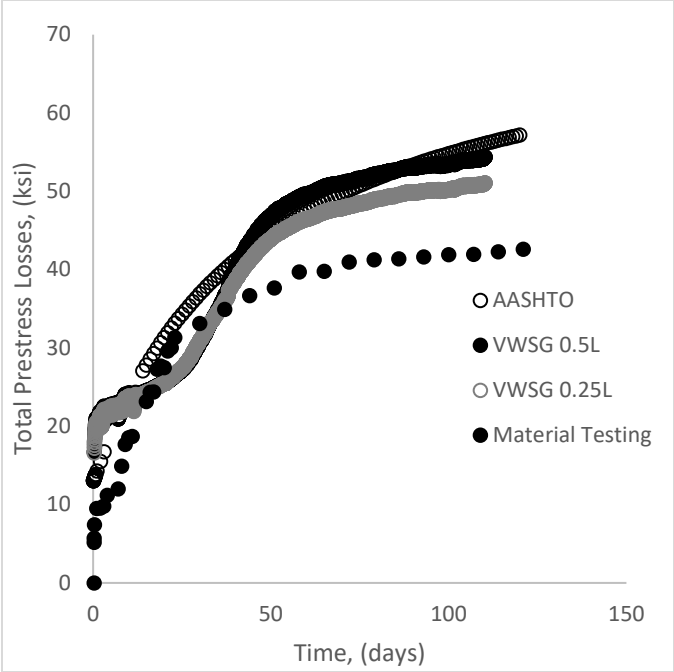

Figure 5.23 Measured Prestress Losses vs. AASHTO Predicted

Prestress losses calculated using AASHTO equations slightly overestimated measured prestress losses from the VWSG data and material testing. Effective prestress was calculated using Equation 5.2 and using strains as measured from various testing of either the beam or the material.

$$f_{pe} = \left(\varepsilon_{pi} - \varepsilon\right) * E_p \tag{5.2}$$

Where:

ε = measured strain, (in./in.)
ε_{pi} = initial strain in the prestressing steel, (in./in.)
E_p = elastic modulus of the prestressing steel, (ksi)

Table 5.2 summarizes calculations of effective prestress for the various testing performed as well as calculated from AASHTO Equation 5.9.5.1-1.

Table 5.2 Effective Prestress Calculations

Method	f_{pe}, (ksi)
VWSG	145.732
Material Testing	149.537
Crack Reopening	138.169
AASHTO	139.078

Effective prestress for CSA cement concrete was higher than the AASHTO predicted value for all measured values of effective prestress except that of the crack reopening test. The average measured effective prestress for CSA cement concrete is 144.5 ksi +/- 5.8 ksi. If the average measured effective prestress is taken as the actual effective prestress, then AASHTO predicts effective prestress for CSA cement concrete with reasonable accuracy for the time period investigated. Based on the material testing, it is likely that the AASHTO equations to estimate prestress losses will overestimate losses long term. Further investigation is warranted.

6. FULL-SCALE MIDSPAN TESTING RESULTS

6.1 Midspan Testing

Midspan testing was carried out as described in Section 3.4.3. A single point load was applied at the midspan in small increments until failure occurred, following the same test setup as the crack initiation and reopening test setups. Load vs. deflection for the midspan test is shown in Figure 6. 1. Strand end-slip was also measured for the midspan test, and the results are summarized in Figure 6.2.

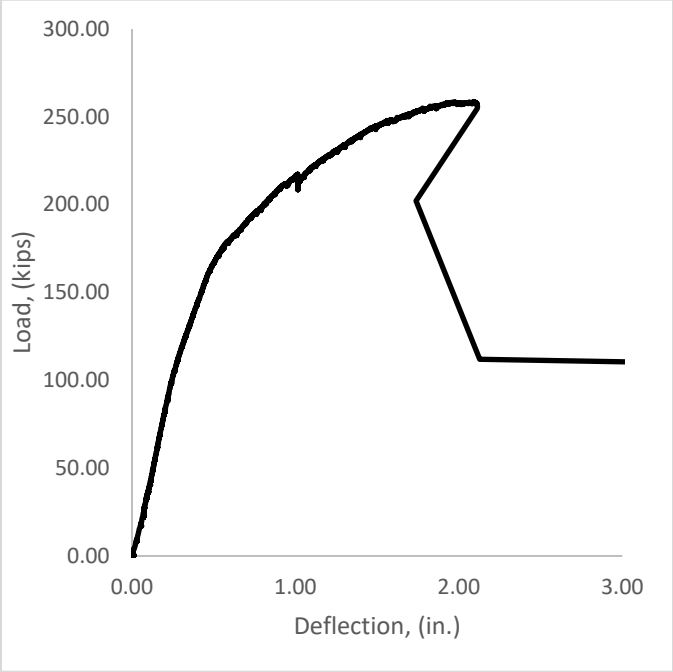

Figure 6.1 Midspan Load vs. Deflection

The maximum load during the midspan test was 258.6 kips, with a corresponding deflection of 2.096 in. The data stop just after the maximum load because the concrete screws that held the wire potentiometers fell out of the concrete due to the violent failure. Figure 6.3 shows the failure of the midspan test.

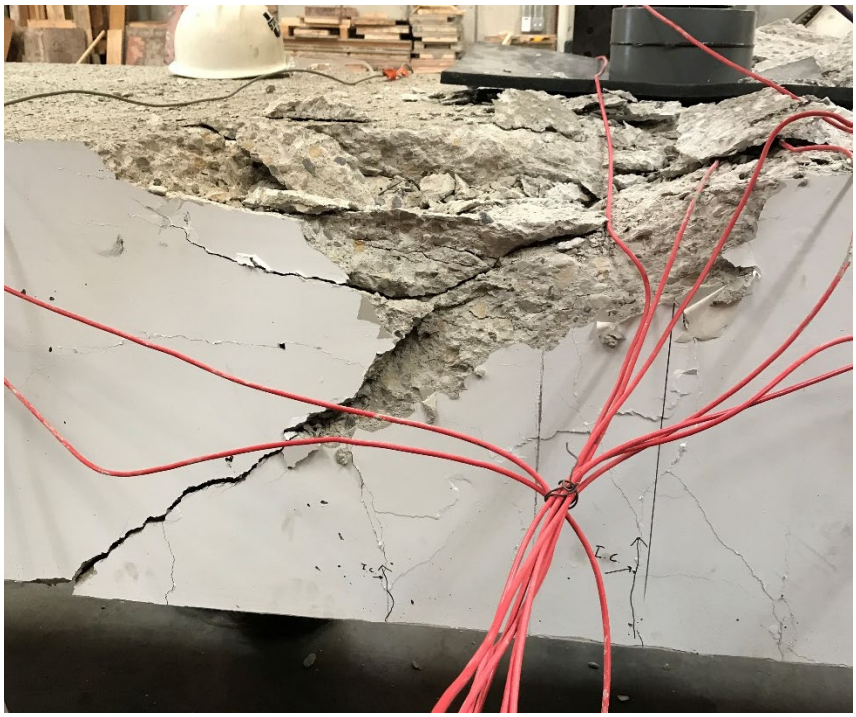

Figure 6.2 Midspan Test Failure Mode

The diagonal cracks and violent failure suggest a shear failure. Embedment length strands was 132 in. AASHTO development length was 104 in. If a bond failure was observed from the midspan test, slip would have been observed. Figure 6.3 shows the strand end-slip as measured during the midspan test. Strand end-slip was not observed, therefore this test most likely resulted in a shear failure. Shear and moment capacity for the actual beam is calculated in the next sections.

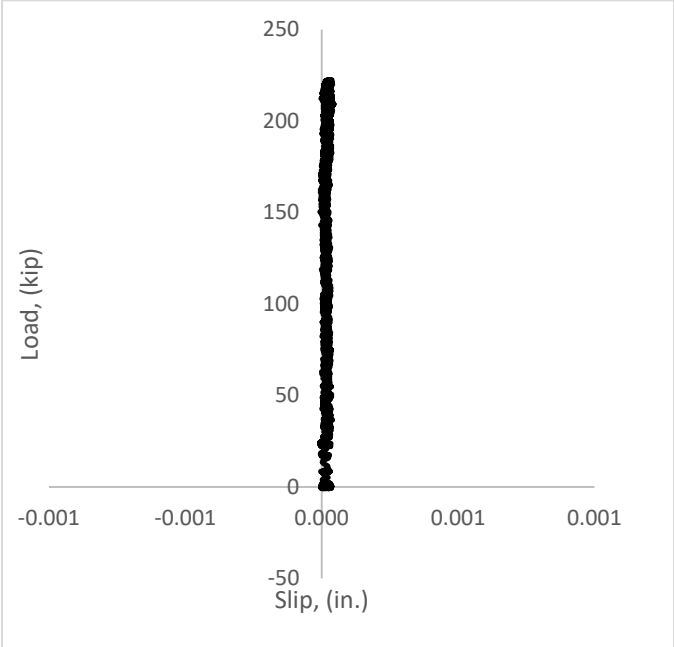

Figure 6.3 Midspan Strand End-slip

6.2 Shear Capacity at Midspan

Midspan shear capacity was calculated and compared with the ultimate load experienced in the test. The ultimate load consisted of the dead weight of the beam, the effective prestress, and the applied point load at the midspan. Shear capacity was calculated according to AASHTO provisions for shear capacity using the V_{ci}/V_{cw} method for shear capacity and simplified modified compression field theory (MCFT). Shear capacity for the V_{ci}/V_{cw} method relies on load factors for parts of the equations, but in order to compare to the test, all load factors were reduced to 1.0.

Shear capacity can be approximated using AASHTO Equation 5.8.3.3-1 and Equation 5.8.3.3-2. These equations are discussed in Chapter 2, and are slightly different depending on whether V_{ci}/V_{cw} or MCFT is used. Table 6.1 summarizes the results of shear capacity at the midspan compared with the measured applied shear from the midspan test.

Table 6.1 Shear Capacity for Midspan Loading

Method	V_n	$V_{applied}$	Measured/ Predicted
AASHTO $V_{ci}V_{cw}$	126.15	129.00	1.023
MCFT	128.90	129.00	1.001

MCFT provided a more accurate prediction for the observed capacity than the V_{ci}/V_{cw} method. However, both methods accurately predicted the shear strength for the CSA cement concrete bridge girder. Therefore, resistance factors for AASHTO LRFD bridge design for concrete beams in shear are accurate based on this limited study.

6.3 Shear Capacity Conclusions

Shear capacity from the actual midspan test was compared with two methods that predict shear capacity: AASHTO V_{ci}/V_{cw} and MCFT in AASHTO. Shear capacity was best predicted using MCFT, as shown by the measured-to-predicted ratios given in Figures 6.1 and 6.2. Because the failure occurred at a value higher than the predicted shear capacity, the midspan test can be considered a shear failure.

Code predicted values of shear capacity are intended to provide an accurate but conservative prediction of shear capacity. That goal was achieved for the voided deck slab made with CSA cement concrete, as seen in Figures 6.1 and 6.2. Therefore, AASHTO provisions for predicting shear capacity in CSA cement concrete are adequate, based on the limited full-scale testing of this study.

6.4 Moment Capacity at Midspan

Moment capacity for the voided deck slab was calculated using a moment curvature analysis. Measured applied moment can be found from statics using the maximum load and length of the span. Figure 6.4 shows the moment curvature analysis using Response 2000.

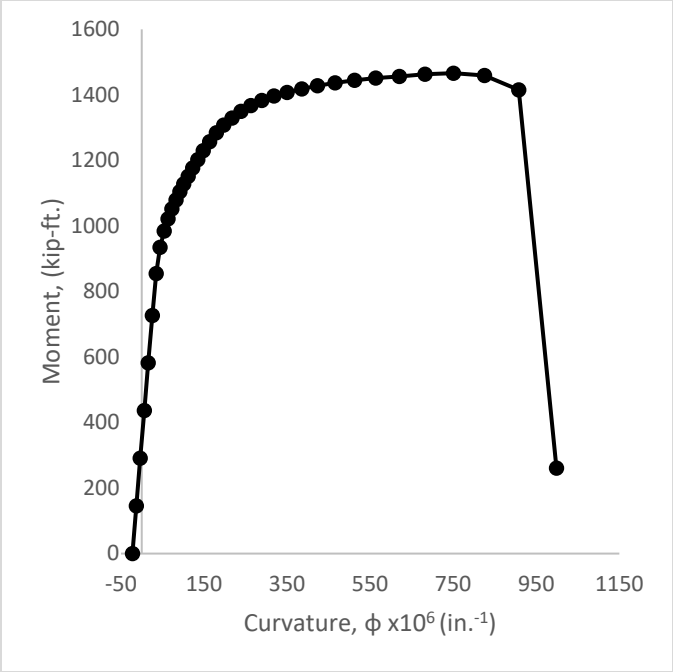

Figure 6.4 Moment Capacity Results

The measured applied moment due to the 258 kip point load was 1,290 kip-ft. The capacity from the moment curvature analysis was 1,466.2 kip-ft., as seen in Figure 6.4. The midspan test resulted in a shear failure without slip in the strands. The calculations also suggest that the member did not fail in flexure, which had a higher predicted strength than with shear.

6.5 Midspan Testing Conclusions

After analysis of the midspan testing, the following conclusions can be made. Maximum applied load at the midspan was 258 kips with a corresponding deflection of 2.096 in. measured directly beneath the load. The maximum applied moment was 1,290 kip-ft., while strain compatibility predicts a value of 1,466.2 kip-ft. and no strand slip was observed during the test. Therefore, the failure at the midspan was not a flexural failure. The maximum applied shear at the midspan was 129.0 kips, while the AASHTO predicted value of shear capacity was 126.2 kips.

The failure at the midspan was due to shear, and AASHTO shear prediction accurately predicted shear capacity in the CSA cement concrete voided slab. Because the midspan test resulted in a shear failure without any observed slip, the development length of the voided deck slab was shorter than the embedment length of the strands.

7. FULL-SCALE 1.25D TESTING RESULTS

7.1 Full-Scale 1.25d Testing

The second portion of the full-scale voided deck slab testing consisted of the destructive testing at a distance 1.25 times the depth of the beam from the face of the support. The testing at 1.25d was carried out on half of the voided deck slab. The testing was carried out as described in Section 3.4.4. The voided deck slab suffered extensive damage from the midspan testing and formed a plastic hinge at the midspan when tested at 1.25d.

In order to remedy the plastic hinge, the voided deck slab was cut in half and simply supported over a span length of 8 ft. 11 in. Figure 7.1 shows the 1.25d test setup. The 1.25d testing was only carried out on the east end of the beam because the west end suffered too much damage from the midspan testing. Figure 7.2 and Figure 7.3 show the failure of the voided deck slab after the 1.25d testing.

Figure 7.1 1.25d Test Setup

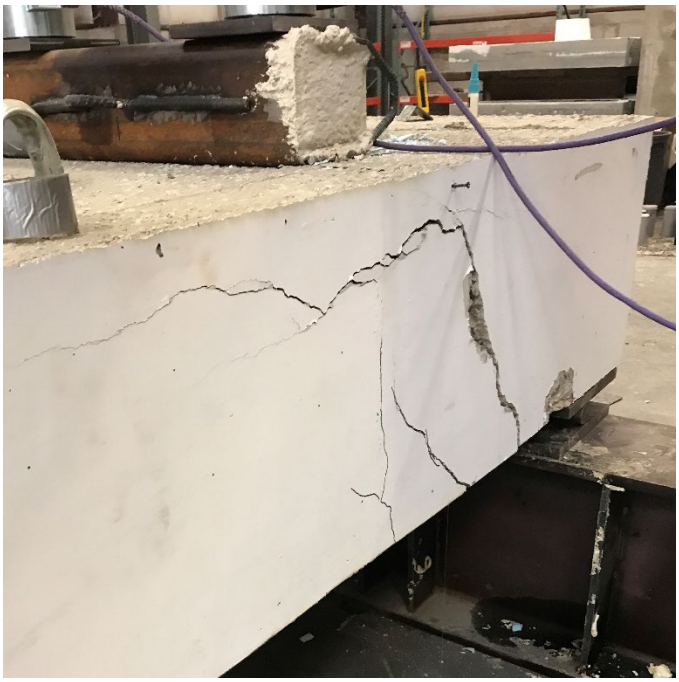

Figure 7.2 Failure of 1.25d Testing North Face

Figure 7.3 Failure of 1.25d Testing South Face

The figures above show cracks forming at nearly 45-degree angles, suggesting a shear failure mode. However, as the crack propagates upward, the crack turns to follow the longitudinal axis of the beam. The longitudinal cracking suggests a bond-slip failure. This chapter discusses the moment and shear capacity of the beam compared with the applied loading and develops a bond-slip model for the voided deck slab.

7.2 Full-Scale 1.25d Testing Results

Full-scale 1.25d testing results are summarized in Figure 7.4 and 7.5. Figure 7.4 summarizes the load vs. deflection results and Figure 7.5 summarizes the load vs. strand end-slip results for the 1.25d testing. Maximum load and deflection at maximum load for the 1.25d testing were 484.9 kips and 0.194 in.

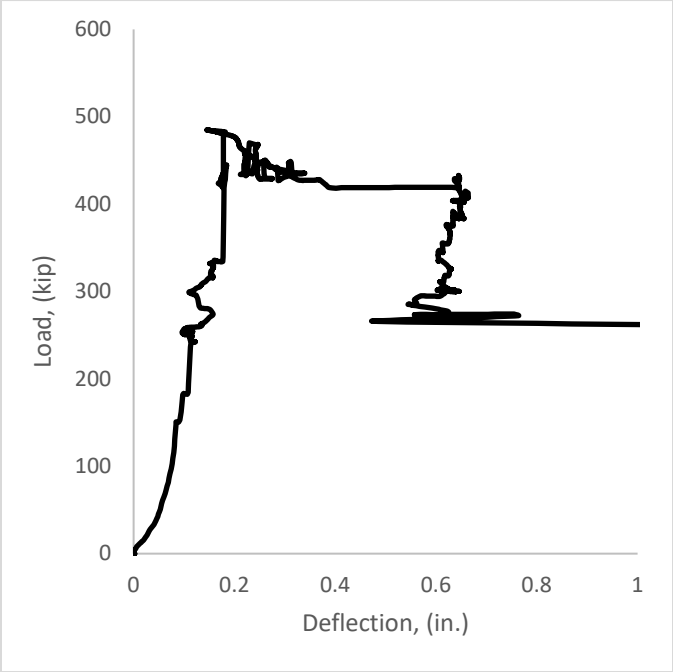

Figure 7.4 Load vs. Deflection for 1.25d Testing

Strand end-slip for midspan testing was essentially zero for the entire duration of the midspan test. However, in the 1.25d testing, strand end-slip was noticeable both graphically, as seen in Figure 7.5, and audibly during the test. The slipping of the strands corresponded to a loud metallic popping sound, followed by a noticeable jump in the slip at the time of the sound. Strand end-slip corresponding to the maximum load of 484.9 kips was 0.0924 in. Final strand end-slip was measured as 0.143 in. after the load was released.

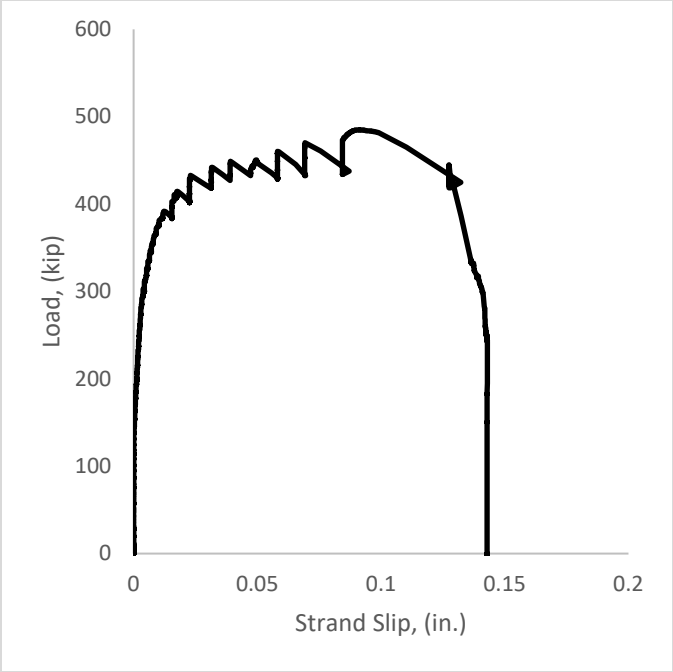

Figure 7.5 Load vs. Strand End-slip for 1.25d Testing

7.3 Moment Capacity at 1.25d

Moment capacity at 1.25d was calculated using a moment curvature analysis and using the bond-slip model. The bond model for the CSA voided deck slab is given in Figure 7.6. The model shows a rapid increase in stress in the strands from the end of the beam to the transfer length, with a slower gain in stress along the development length.

The ultimate stress in the strands was found by performing a strain compatibility analysis and by using the power formula for calculating stress in the strands. The value of f_{ps} given in the bond model represents the maximum stress in the strands at any location along the beam. Exceeding the maximum stress in the strands results in bond failure between the strands and the concrete. This maximum f_{ps} is compared with the f_{ps} measured in the strands due to the loading. The stress in the strands from the measured load was calculated using the power formula and the sum of forces and moments to find the concrete strain and value of "c". A bond-slip failure occurs when the stress in the strands exceeds the maximum stress as given in the bond model.

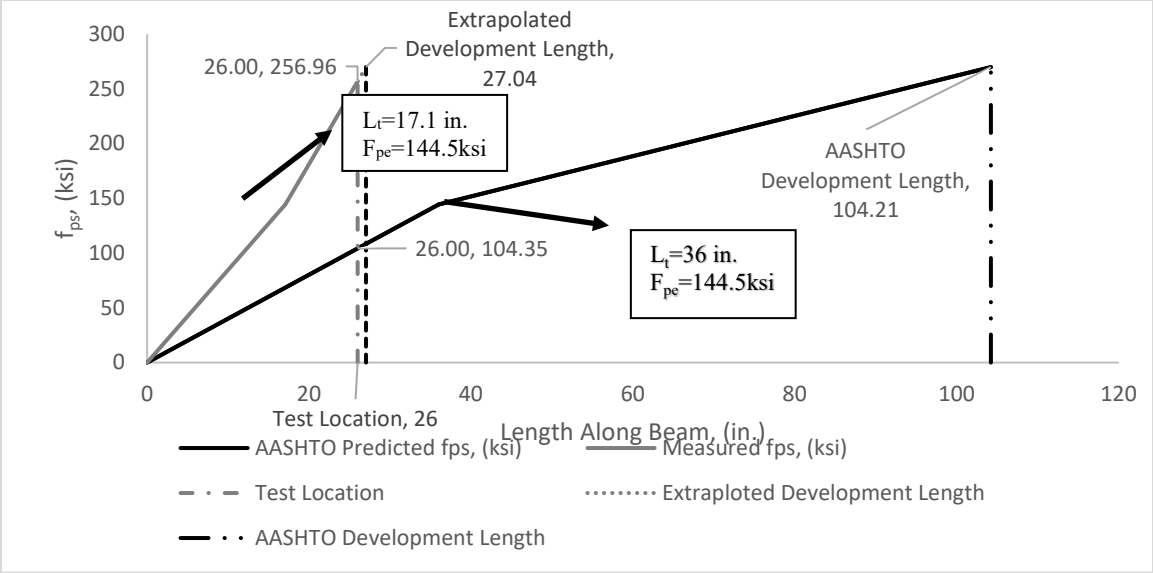

Figure 7.6 Bond Model for Voided Deck Slab

The bond-slip model developed in Figure 7.6 compares the AASHTO development length model with the measured development and transfer length. The measured stress in the strands due to the maximum applied load of 484.9 kips at the test location was measured as 256.96 ksi. The AASHTO model predicts the stress capacity in the strands as 104.35 ksi. The measured development length can be extrapolated using the measured stress in the strands and is given in Figure 7.6 as 27.04 in. AASHTO predicts the development length to be 104.21 in.

7.4 Shear Capacity at 1.25d

Shear capacity at midspan was unable to be correctly calculated using traditional methods for shear capacity calculations. According to Schlaich et al. 1991, shear capacity near the end of a beam may be better approximated by creating a strut-and-tie model. The strut-and-tie model accounts for the truss-like behavior of a concrete member near the supports. The strut-and-tie model for the 1.25d test can be found in Appendix A. Shear capacity was calculated to be 700 kips according to the strut-and-tie model, compared with the applied shear of 367 kips from the 1.25d test. Based on the visually observed failure mode, measured slip in the strands during the test, and the strut-and-tie model strength prediction, the 1.25d test resulted in a flexural bond failure.

7.5 Full-Scale 1.25d Testing Conclusions

Full-scale testing at the 1.25d location resulted in a bond-slip failure of the concrete. This was made evident when the stress in the strands exceeded the allowable stress as seen in the bond model, and because the shear capacity was calculated to be 700 kips compared with the applied shear of 484.9 kips. The bond capacity at the point of the test according to AASHTO is 104.35 ksi, compared with the measured capacity of 256.96 ksi.

8. CONCLUSIONS

8.1 Summary

CSA cement concrete was used in the casting of a prestressed voided deck slab. In order to pour the concrete without the concrete setting, extensive lab mixing of CSA cement concrete was performed in order to find the desired combination of one-hour set-time and initial concrete compressive strength of 4300 psi. The concrete pour of the voided deck slab was performed at Olympus Precast in Bluffdale, Utah. At the time of the concrete pour, compressive cylinders, set-time molds, and drying and autogenous shrinkage molds were made to measure early-age and long-term material properties. Dynamic elastic modulus was also measured at the precast plant. Vibrating wire strain gages were cast into the concrete to measure the long-term prestress losses and temperature changes inside the beam.

The second phase of the study consisted of material property testing of the CSA cement concrete, which was performed in the laboratory at Utah State University. Material testing of CSA cement concrete consisted of compressive and tensile strength, static elastic modulus, dynamic elastic modulus, drying shrinkage, autogenous shrinkage, and creep testing. The results from the shrinkage and creep tests were compared with the AASHTO predicted values for shrinkage and creep strain.

The third phase of this study was the full-scale testing of the voided deck slab. The voided deck slab was tested at the midspan by performing a crack reopening test until failure. Testing was also performed at a location 1.25 times the depth of the beam from the face of the support until failure. Capacity for shear and moment for both the midspan and 1.25d testing were compared with AASHTO predicted values.

8.2 CSA Cement Concrete Mixing Conclusions and Guidelines

After experiencing difficulties achieving the desired set-time and compressive strength of the concrete at four hours, the following conclusions can be made:

- When mixing CSA cement concrete, the admixtures, including superplasticizer, air entrainment, and retarder, must be mixed into the water before cement is added to the drum.
- Half of the water, including the admixtures, must be added to the aggregates before cement is added. If no water is in the mixer when CSA cement is added, the hydration of the cement begins as soon as water is added.

When mixing CSA cement concrete, adhering to the following guidelines will help ensure that there is no flash-setting of the concrete in the mixer.

- Place coarse and fine aggregates into the mixer and add 50% of the water/admixture mixture.
- Allow aggregates and water/admixture to mix thoroughly.
- Begin adding CSA cement and water in equal proportions, leaving about 10% of water after all cement is in the mixer to clean off the sides of the mixer.

8.3 Prestress Losses Conclusions

After measuring time-dependent properties of concrete including creep and shrinkage, the following conclusions can be made about the prestress losses from time-dependent properties of CSA cement concrete:

- Creep strains are accurately predicted using AASHTO for CSA cement concrete under laboratory conditions: 50% humidity and 70° Fahrenheit. AASHTO predictions are likely to overestimate creep strains for times in excess of those studied herein.

- Shrinkage strains are overestimated for CSA cement concrete by AASHTO in the long term, but short-term shrinkage losses are underestimated. However, short-term losses are measured in the lab with autogenous shrinkage, which does not include aggregates. However, because autogenous shrinkage is so large with CSA cement, it may be important to include this behavior when estimating losses. A better test must be designed for autogenous shrinkage that includes large aggregate to accurately measure autogenous shrinkage for this purpose.
- The effective prestress value based solely on the material testing was 149.5 ksi, a value higher (i.e., less losses) than would be predicted by AASHTO predicted value of 139.1 ksi.
- In the voided slab, VWSG measured prestress losses (145.7 ksi) are less than the predicted value using the AASHTO loss prediction equations (139.1 ksi).
- The steep gain in prestress loss at day 20 in the voided slab member's VWSG measured losses most likely comes from the movement of the voided slab off of its original supports.
- Effective prestress measured from the crack reopening test was 138.2 ksi, very close to the AASHTO value of 139.1 ksi.
- The VWSG measurements in the voided slab indicate that for CSA concrete bridge members the AASHTO equations will likely overestimate losses in the long-term (underestimate total effective prestressing) and underestimate losses in the short-term (i.e., overestimate total effective prestressing).

8.4 Full-Scale Midspan Testing Conclusions

After testing the voided deck slab at the midspan, the following conclusions can be made:

- Maximum applied load at the midspan was 258 kips with a corresponding deflection of 2.096 in. measured directly beneath the load, and a shear failure was observed.
- No strand-end-slip was measured during the midspan testing. Therefore, a bond failure did not occur in the midspan test.
- The maximum applied moment was 1,290 kip-ft., while strain compatibility predicted a value of 1,466.2 kip-ft. Based on this calculation, the observed shear failure (and its prediction) and the lack of slip during the test, the development length for the strand was less than the embedment length (132 in.) for the midspan test.
- The maximum applied shear at the midspan was 129.0 kips, while the AASHTO predicted value of shear capacity was 126.2 kips. Modified compression field theory predicted a shear capacity of 128.9 kips. The AASHTO MCFT and Vci/Vcw shear prediction approaches can accurately predict shear capacity of CSA cement concrete members.

8.5 Full-Scale 1.25d Testing Conclusions

After performing full-scale testing of the voided deck slab at a distance 1.25d from the face of the support, the following conclusions can be made:

- A bond-slip failure occurred for the 1.25d test, as made evident by the bond-model shown in Section 7.5. Bond stress capacity according to AASHTO is 104.35 ksi, compared with the test-implied maximum stress of 256.96 ksi in the strand.

8.6 Recommendations for Future Study

Due to the limited scope of this study, more research is needed to validate the results found. A more comprehensive full-scale testing program should be developed in order to compare losses and strength behavior of CSA cement concrete in prestressed concrete applications. More than one specimen should be tested to obtain more reliable results. The length of the specimens is recommended to be longer than the voided slab used in this study in order to conduct shear tests at the ends of the beam, as well as multiple flexural tests on a single beam.

The recommended procedure for mixing CSA cement concrete must be used in order to create repeatable results and a more effective concrete mix. If possible, CSA cement concrete should be cast in a relatively temperature controlled environment, as high temperatures may lead to flash-setting and low temperatures lead to a longer set-time. CSA cement concrete should also be mixed for longer than 90 seconds in order to activate all the admixtures and obtain a workable concrete mix without adding water.

A series of concrete mix designs should be developed in order to serve the need for variable set-time and release strength of concrete requirements. These mix designs should be subject to a thorough material testing program, with results between mix design compared with each other and current design provisions.

REFERENCES

AASHTO LRFD Bridge Design Specifications. Washington, DC: American Association of State Highway and Transportation Officials, 2010. Print.

ACI Committee 318. Building Code Requirements for Structural Concrete: (ACI 318-14); and Commentary (ACI 318R-14). Farmington Hills, MI. American Concrete Institute, 2014. Print.

ASTM C1698-14, Standard Test Method for Autogenous Strain of Cement Paste and Mortar, ASTM International. West Conshohocken, PA, 2014, www.astm.org

ASTM C39 / C39M-18, Standard Test Method for Compressive Strength of Cylindrical Concrete Specimens, ASTM International. West Conshohocken, PA, 2018, www.astm.org

ASTM C403 / C403M-16, Standard Test Method for Time of Setting of Concrete Mixtures by Penetration Resistance, ASTM International, West Conshohocken, PA, 2016, www.astm.org

ASTM C469 / C469M-14, Standard Test Method for Static Modulus of Elasticity and Poisson's Ratio of Concrete in Compression, ASTM International. West Conshohocken, PA, 2014, www.astm.org

ASTM C496 / C496M-17, Standard Test Method for Splitting Tensile Strength of Cylindrical Concrete Specimens, ASTM International. West Conshohocken, PA, 2017, www.astm.org

ASTM C512 / C512M-15, Standard Test Method for Creep of Concrete in Compression, ASTM International. West Conshohocken, PA, 2015, www.astm.org

ASTM C596-09(2017), Standard Test Method for Drying Shrinkage of Mortar Containing Hydraulic Cement, ASTM International, West Conshohocken, PA, 2017, www.astm.org

ASTM C617 / C617M-15, Standard Practice for Capping Cylindrical Concrete Specimens, ASTM International. West Conshohocken, PA, 2015, www.astm.org

Barr, P., Kukay, B. M., Halling, M. W. (2008). "Comparison of Prestress Losses for a Prestressed Concrete Bridge Made with High-Performance Concrete." *Journal of Bridge Engineering*. September 2008, pp. 468-475.

Bentz, E., Vecchio, F., Collins, M. (2006). "Simplified Modified Compression Field Theory for Calculating Shear Strength of Reinforced Concrete Elements." *ACI Structural Journal*, 103, 614-624.

Bescher, E., Stremfel, J., and Ramseyer, C. (2012) "The Role of Calcium Sulfoaluminate in Concrete Sustainability." Twelfth International Conference on Recent Advances in Concrete Technology and Sustainability Issues. Prague, Czech Republic.

Bowser, T. (2016). "Development Length of 0.6 in. Prestressing Strands in Precast, Prestressed Calcium Sulfoaluminate Cement Concrete." University of Oklahoma, Norman, OK.

Carroll, J. (2009). "Grade 300 Prestressing Strand and the Effect of Vertical Casting Position." Virginia Polytechnic Institute and State University, Blacksburg, VA.

Cross, B. (2012). "Structural Performance of High Strength Lightweight Concrete Pretensioned Bridge Girders." Virginia Polytechnic Institute and State University, Blacksburg, VA.

Gross, S., Burns, N. H. (1995). "Transfer and Development Length of 15.2 mm (0.6 in.) Diameter Prestressing Strand in High Performance Concrete: Results of the Hoblitzell-Buckner Beam Tests." Center for Transportation Research, University of Texas at Austin, Austin, TX.

Guyon, Y. (1960). Prestressed Concrete. John Wiley & Sons, New York.

Hanson, N. W., and Kaar, P. H. (1959). "Flexural Bond Tests of Pretensioned Prestressed Beams." *ACI Journal*, 30(7), 783-802.

Hargis, C.W., Telesca, A., and Monteiro, P.J.M. "Calcium Sulfoaluminate (Ye'elimite) Hydration in the Presence of Gypsum, Calcite, and Vaterite." *Cement and Concrete Research*, V. 65, Nov. 2014, pp. 15-20.

Janney, J. R. (1954). "Nature of Bond in Pre-tensioned Prestressed Concrete." *Journal of the American Concrete Institute*, 25(9), pp. 717-736.

Kassner, B. (2012). "Shear Strength of Full-Scale Prestressed Lightweight Concrete Girders with Composite Decks." Virginia Polytechnic Institute and State University, Blacksburg, VA.

Kim, Young Hoon. "Flexural Behavior of High-Early-Strength Self-Consolidating Concrete Pretensioned Bridge Girders: Experimental Evaluation."

Lin, T.Y. *Design of Prestressed Concrete Structures. 2nd ed*. New York, NY: Wiley, 1955.

Maguire, M. (2009). "Impact of 0.7 inch Diameter Prestressing Strands in Bridge Girders." University of Nebraska, Lincoln, NE.

Maguire, M., Morcous, G., and Tadros, M. (2013) "Structural Performance of Precast/Prestressed Bridge Double-Tee Girders Made of High-Strength Concrete, Welded Wire Reinforcement, and 18-mm-Diameter Strands" *ASCE Journal of Bridge Engineering*, 18(10), 1053-1061.

Marti-Vargas, J. R., Arbelaez, C. A., Serna-Ros, P., and Castro-Bugallo, C. (2007). "Reliability of Transfer Length Estimation from Strand End-slip." *ACI Structural Journal*, 104(4), 487-494.

Naaman, Antoine E. *Prestressed Concrete Analysis and Design: Fundamental. 3rd ed*. Ann Arbor, MI: Techno Press 3000, 2012.

Péra, J. (2004). "New Applications of Calcium Sulfoaluminate Cement." Institut National des Sciences Applique´es de Lyon, Cedex, France.

Pettigrew, Christopher S., "Flexural, Shear, and Punching Shear Capacity of Three 48-Year-Old Prestressed Lightweight Concrete Double-Tee Bridge Girders." (2014). All Graduate Theses and Dissertations. 3852. https://digitalcommons.usu.edu/etd/3852

Pettigrew, C., Barr, P., Maguire, M., and Halling, M. (2016) "Behavior of 48-Year-Old Double-Tee Bridge Girders Made with Lightweight Concrete." *ASCE Journal of Bridge Engineering*. 21(9). 1-11.

Schaich, J., and Schäfer, K. (1991). "Design and Detailing of Structural Concrete Using Strut-and-Tie Models." *The Structural Engineer*, V. 69 March 1991, pp. 113-125.

Tadros, M. K., Al-Omaishi, N., Seguirant, S. J., and Gallt, J. G. (2003). "Prestress Losses in Pretensioned High-Strength Concrete Bridge Girders." NCHRP Report 496, Transportation Research Board, Washington, DC.

Thomas, R., Maguire, M., Sorensen, A., Quezada, Ivan (2018). "Calcium Sulfoaluminate Cement: Benefits and Applications." *Concrete International*, V. 40 April 2018, pp. 65-69.

Wilden, Helmuth. *PCI Design Handbook: Precast and Prestressed Concrete*. Chicago: Precast/Prestressed Concrete Institute, 2010. Print.

Winnefeld, F. (2009). "Hydration of Calcium Sulfoaluminate Cements - Experimental Findings and Thermodynamic Modeling." Swiss Federal Laboratories for Materials Testing and Research, Dübendorf, Switzerland.

Zajac, M., Skocek, J., Bullerjahn, F., and Haha, M.B. “Effect of Retarders on the Early Hydration of Calcium-Sulpho-Aluminate (CSA) Type Cements,” *Cement and Concrete Research*, V. 84, June 2016, pp. 62-75.